Taylor & Francis
Taylor & Francis Group

CLINICAL RESEARCH PAPER

◌ OPEN ACCESS

Autophagy orchestrates adaptive responses to targeted therapy in endometrial cancer

Núria Eritja[a,b,#], Bo-Juen Chen[c,#], Ruth Rodríguez-Barrueco[d,#], Maria Santacana[a,b], Sònia Gatius[a,b], August Vidal[e], Maria Dolores Martí[f], Jordi Ponce[f], Laura Bergadà[a,b], Andree Yeraman[a,b], Mario Encinas[g], Joan Ribera[g], Jaume Reventós[e,f], Jeff Boyd[h], Alberto Villanueva[i], Xavier Matias-Guiu[a,b,e,f,$], Xavier Dolcet[a,b,$], and David Llobet-Navàs ◌[d,$]

[a]Department of Basic Sciences, Universitat de Lleida/Institut de Recerca Biomèdica de Lleida, Edifici Biomedicina I, Lab 2.4, Lleida, Spain; [b]Department of Pathology, Universitat de Lleida/Institut de Recerca Biomèdica de Lleida/Hospital Universitari Arnau de Vilanova, Lleida, Spain; [c]New York Genome Center, New York, NY, USA; [d]Institute of Genetic Medicine, Newcastle University, Newcastle-Upon-Tyne, UK; [e]Department of Pathology, University Hospital of Bellvitge, Bellvitge Biomedical Research Institute (IDIBELL), L'Hospitalet de Llobregat, Barcelona, Catalonia, Spain; [f]Department of Gynecology, University Hospital of Bellvitge, Bellvitge Biomedical Research Institute (IDIBELL), L'Hospitalet de Llobregat, Barcelona, Catalonia, Spain; [g]Department of Experimental Medicine, Universitat de Lleida/Institut de Recerca Biomèdica de Lleida, Edifici Biomedicina I, Lab 2.8, Lleida, Spain; [h]Department of Human and Molecular Genetics, Herbert Wertheim College of Medicine, Florida International University, Miami, FL, USA; [i]Chemoresistance and Predictive Factors Group, Program Against Cancer Therapeutic Resistance (ProCURE), Catalan Institute of Oncology (ICO), Bellvitge Biomedical Research Institute (IDIBELL), L'Hospitalet de Llobregat, Barcelona, Catalonia, Spain

ABSTRACT

Targeted therapies in endometrial cancer (EC) using kinase inhibitors rarely result in complete tumor remission and are frequently challenged by the appearance of refractory cell clones, eventually resulting in disease relapse. Dissecting adaptive mechanisms is of vital importance to circumvent clinical drug resistance and improve the efficacy of targeted agents in EC. Sorafenib is an FDA-approved multitarget tyrosine and serine/threonine kinase inhibitor currently used to treat hepatocellular carcinoma, advanced renal carcinoma and radioactive iodine-resistant thyroid carcinoma. Unfortunately, sorafenib showed very modest effects in a multi-institutional phase II trial in advanced uterine carcinoma patients. Here, by leveraging RNA-sequencing data from the Cancer Cell Line Encyclopedia and cell survival studies from compound-based high-throughput screenings we have identified the lysosomal pathway as a potential compartment involved in the resistance to sorafenib. By performing additional functional biology studies we have demonstrated that this resistance could be related to macroautophagy/autophagy. Specifically, our results indicate that sorafenib triggers a mechanistic MAPK/JNK-dependent early protective autophagic response in EC cells, providing an adaptive response to therapeutic stress. By generating in vivo subcutaneous EC cell line tumors, lung metastatic assays and primary EC orthoxenografts experiments, we demonstrate that targeting autophagy enhances sorafenib cytotoxicity and suppresses tumor growth and pulmonary metastasis progression. In conclusion, sorafenib induces the activation of a protective autophagic response in EC cells. These results provide insights into the unopposed resistance of advanced EC to sorafenib and highlight a new strategy for therapeutic intervention in recurrent EC.

Introduction

Endometrial cancer (EC) is the most common gynecologic malignancy in the Western world with more than 280,000 cases per year worldwide.[1,2] The incidence of EC has increased by 21% since 2008 and about one in 37 women will develop it during their lifetime.[2,3]

Histological and pathological evaluation classifies EC into type I (endometrioid) and type II (nonendometrioid) tumors (Bokhman's classification).[4] Type I ECs are low grade, estrogen-

dependent tumors that originate from pre- or peri-menopausal women. Type II ECs are very aggressive, estrogen-independent tumors that arise in older women and present a worse outcome when compared with type I lesions. Recently, a new classification based on molecular profiling of EC has shed light into the different genomic subtypes of EC with the potential to improve and predict new postsurgical adjuvant treatments.[5]

Prognosis for EC at early stages, when primary surgical resection is often curative, is excellent, leading to 5-y survival

---

rates of over 70%. Unfortunately, 15–20% of EC cases recur after surgery to vaginal or pelvic regions, often metastasizing to distant sites.[6,7] Patients showing high-risk tumor features (high grade, deep myometrial invasion, cervical involvement) receive adjuvant radiation, chemotherapy or both. However, these treatments are estimated to benefit only 10–15% of all patients.[8]

Consequently, the prognosis of patients with recurred or advanced (metastatic) EC is poor with median survival rates of less than one y.[9] Current response rates to molecularly targeted drugs are poor in relapsed EC and the urge for the development of improved targeted therapies has become one of the major concerns.
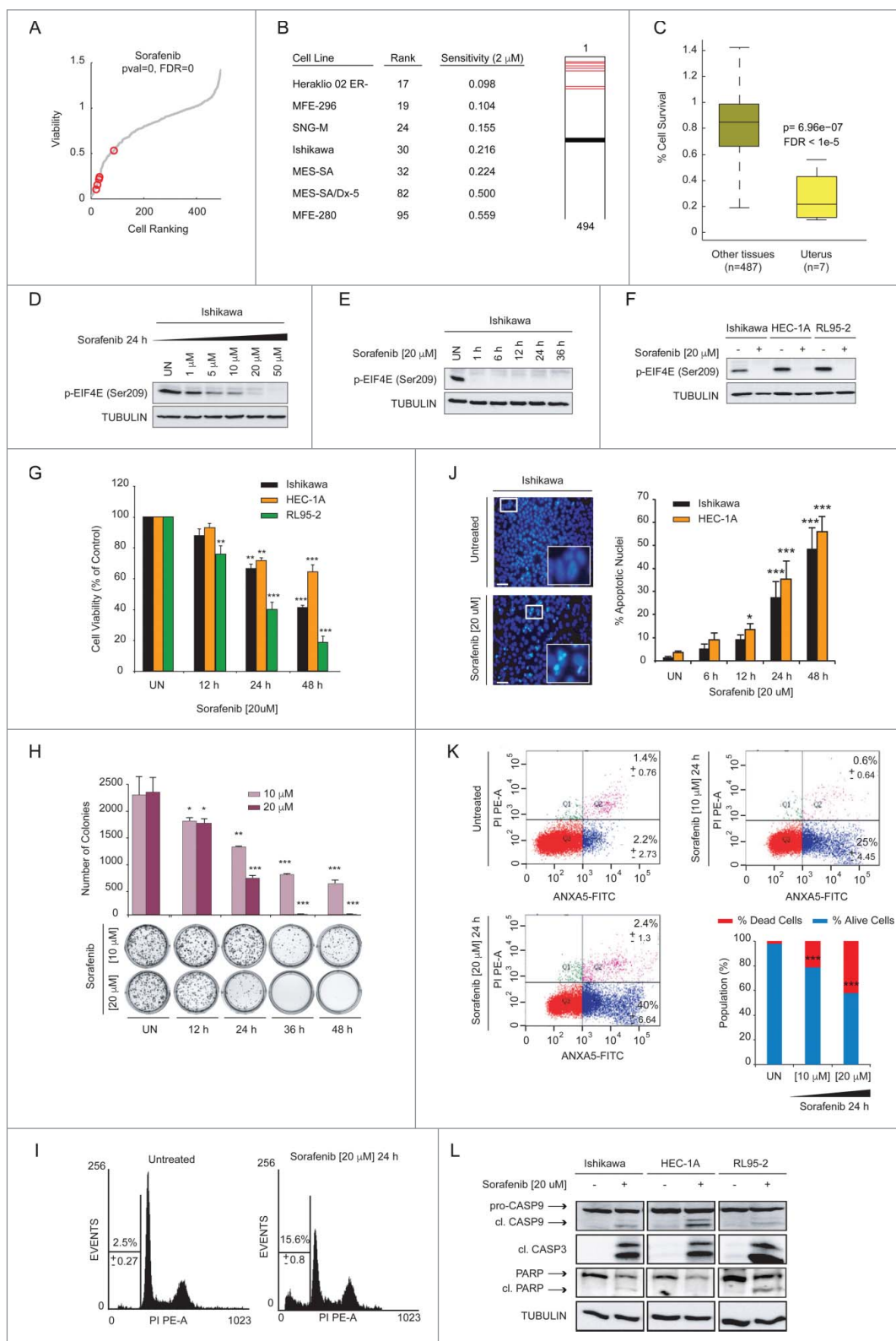

Figure 1. (For figure legend, see page 610)

In recent years, structural and functional evidence has pointed to tyrosine kinases (TKs) as essential components of tumor progression by sustaining proliferation/survival of cancer cells, and thus represent a major pharmaceutical target against cancer.[10-12] Unbalanced kinase signaling has primed the development of molecularly driven targeted compounds aimed at reducing toxicity and for tailored adjuvant and neoadjuvant treatments.

Sorafenib (BAY 43–9006, Nevaxar) is a broad-spectrum kinase inhibitor with antiangiogenic properties currently administered in patients with advanced renal cell carcinoma, hepatocellular carcinoma and most recently in metastatic thyroid carcinoma.[13,14] Sorafenib was initially designed to inhibit RAF1, but subsequent studies revealed that its inhibitory action expanded to other intracellular kinases such as BRAF and prominent receptor tyrosine kinases (RTKs) such as KDR, FLT4, KIT, FGFR1, PDGFRA and RET.[15,16] Because of its antiangiogenic properties, sorafenib has been proposed as a promising targeted therapy for EC. Several lines of evidence supported this rationale (e.g., the prominent role of the RAS-RAF-MAP3K/MEK-MAPK pathway or the increased levels of VEGFA and angiogenic markers in EC patients).[17-19] Unfortunately, very modest effects were observed in a multicenter phase II trial when tested in advanced uterine carcinoma patients.[20] In the present study we dig into the mechanistic basis of this resistance and introduce a new approach to improve sorafenib efficacy in EC patients.

Results

Sorafenib targets EC cells with high specificity

Given the poor clinical benefits of sorafenib observed in EC patients we re-evaluated the efficacy of sorafenib in EC. To address this, we reanalyzed the effects of a panel of TK inhibitors, including sorafenib, in a high-throughput screening using 494 cancer cell lines.[21] We focused our analysis on 12 selective kinase inhibitors with sensitivity data for EC cell lines. For each drug we ranked cancer cell lines according to their sensitivity and tested if EC cell lines are over-represented among sensitive cell lines (based on gene set enrichment analysis [GSEA], see Materials and Methods).[22] Our analysis revealed that sorafenib was the most effective compound compromising EC cell viability (Figs. 1A-C, S1A and S1B). We further explored the effects of sorafenib on EC cells by analyzing the ability of sorafenib to decrease the levels of phosphorylated (p-)EIF4E, a hallmark of sorafenib's mechanism of action.[23-29] Our data indicated that sorafenib treatment resulted in a dramatic decrease in p-EIF4E levels (Fig. 1D-F) and compromised EC cell viability and clonogenic capabilities (Fig. 1G and 1H) by inducing cellular DNA loss (Fig. 1I), increasing the number of apoptotic cells (Fig. 1J and K) and triggering caspase activation and PARP (poly[ADP-ribose] polymerase) proteolysis in different EC cell lines (Fig. 1L). These results point to sorafenib being an effective anticancer agent against EC cells in vitro and support previous observations.[30,31]

Sorafenib induces macroautophagy in EC cells

The discrepancy between our data obtained in vitro and the poor effects of sorafenib in EC patients prompted us to dissect the underlying mechanisms of this resistance. The mechanistic dissection of this phenomenon could entail instrumental insights that could result in clinical benefits. Previous attempts to potentiate sorafenib activity have shown that modulation of antiapoptotic proteins such as CFLAR/FLIP, BCL2L1/BCL⁻XL, BCL2 or MCL1 can increase sorafenib cytotoxic activity.[30-33] To explore the genetic program associated with sorafenib resistance, we used GSEA to test the association between gene expression signatures and sensitivity to sorafenib (see Methods).[34] Interestingly, we found significant enrichment of genes encoding lysosomal and catabolic metabolism pathway components among those whose expression negatively correlated with sorafenib sensitivity (Figs. 2A and S2A-S2D).

The lysosomal compartment represents one of the main cellular pathways implicated in the degradation of all sorts of macromolecules. Importantly, lysosomes play prominent roles in cell secretion, signaling and energy metabolism processes with the potential to influence drug response functions.[35] Based on this, we hypothesized that lysosomal activity could be involved in the resistance to sorafenib in our experimental model and could be used as a first-line approach to further dig into this phenomenon. First, to study the effects of sorafenib on lysosomal function we used a fluorescent acidotropic probe highly selective for lysosomes to measure pH-dependent changes in fluorescence intensity upon acidification. Our data showed an increase in fluorescence after sorafenib treatment in EC cells, indicative of a progressive cellular acidification (Fig. S2E). Correct lysosomal acidification is essential to facilitate the digestion of cellular components via the endocytic or the autophagic pathways.[36] On the basis of these lines of evidence and given the role of autophagy as a cellular mechanism to cope with therapeutic stress,[37] we aimed to determine whether sorafenib triggered a cellular autophagic response, a phenomenon that

Figure 1. (see previous page) Sorafenib targets endometrial cancer cells with high specificity and induces apoptotic cell death. (A) Analysis of sorafenib effects in a high-throughput screening using kinase inhibitors in a panel of 494 cancer cell lines[21] Sensitivity was calculated as the fraction of viable cells relative to untreated controls following treatment with 2μM sorafenib for 72 h[21]. The sensitivity values of cell lines are plotted as a function of the ranking of the sensitivity (from sensitive to resistant). Uterus cell lines (red circles) are over-represented among sensitive cell lines. (B) Left, ranking and sensitivity of $_{EC}$ cells to sorafenib among the 494 cancer cell lines. Right, graphical representation of the ranks, according to decreasing order of sensitivity, among the 494 cell lines analyzed. EC cells are represented as red lines in the top half of the ranking. Thick bar represents the median rank. (C) Box plot illustrating sorafenib effects in the uterus (n cell lines = 7) compared with the rest of the tissues (18 other tissues, n cell lines = 487). P-value = 6.96e-7 (FDR<1e-5, t-test). For additional information please see Fig. S2B. Other tissues include bladder, skin, bone, brain, lung, stomach, kidney, thyroid, ovary, pancreas, breast, esophagus, cervix, intestine and liver. Sorafenib effects were assessed in vitro by measuring p-EIF4E levels by western blot in a dose-dependent treatment (D) and a time-course treatment (E) in Ishikawa cells. Results were further validated in 2 independent EC cell lines (HEC-1A and RL95–2) at final concentration (F). Western blot against tubulin was performed to ensure equal protein loading amounts. MTT assays in Ishikawa, HEC-1A and RL95–2 cells (G) and clonogenicity assays in Ishikawa cells (H) were performed to measure sorafenib effects on cell viability. Values are represented as the percentage of viable cells or colonies compared with untreated cells. Sorafenib-induced apoptosis after 24 h of treatment was characterized by measuring DNA fragmentation by flow cytometry (sub G₁ phase) (I), quantifying pyknotic nuclei by Hoechst staining (J) and analysis of ANXA5/Annexin V-positive cells by flow cytometry (K) in Ishikawa cells. (L) Western blot showing activation of inducer CASP9, executioner CASP3 and PARP cleavage after sorafenib 20μM treatment of 24 h in different EC cell lines. All experiments were performed in triplicate. T test statistical significant differences were calculated by comparison to untreated conditions. *$p < 0.05$, **$p < 0.01$, ***$p < 0.001$. Scale bar: 100μM.

has been previously reported in other cell types.[33,38-42] To accomplish these goals we first monitored the conversion of soluble MAP1LC3B/LC3B (LC3B-I) by western blot to phosphatidylethanolamine-modified LC3B (LC3B-II), an autophagosome-associated molecule and a hallmark of autophagy. We observed an increase in lipidated LC3B in Ishikawa, HEC-1A and KLE cells after 12 h of sorafenib (20 μM) treatment

(Fig. 2B) and at different concentrations and over time (Fig. S2F and S2G). These results suggest an increase in autophagosome formation in response to sorafenib. Notably, LC3B-I to LC3B-II conversion was observed as early as 12 h after treatment while the effects of sorafenib on cell viability at this time point were barely detectable (Fig. 1G and 1H) and the apoptotic rate in Ishikawa cells remained below 10% (Fig. 1J),
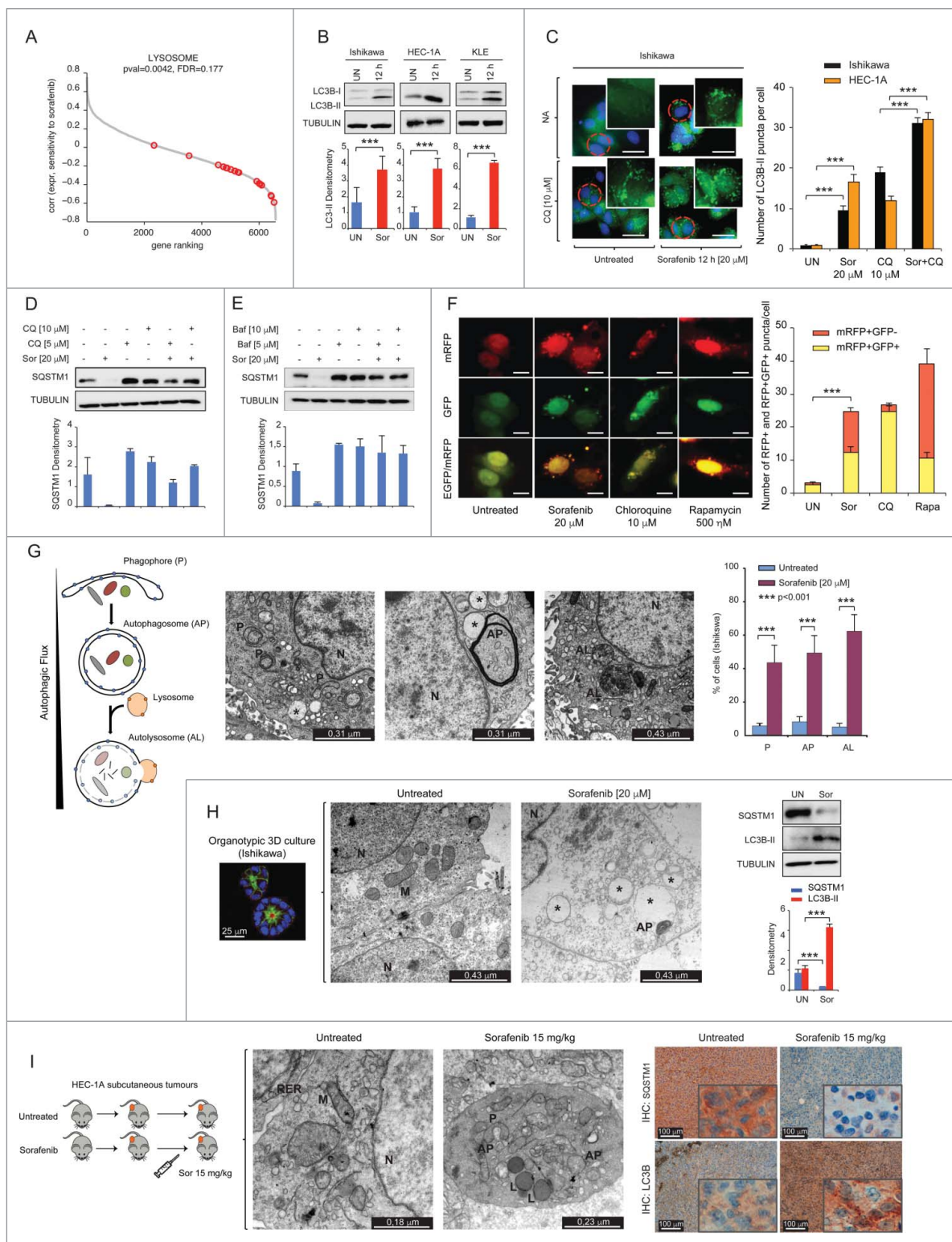

Figure 2. (For figure legend, see page 612)

indicating that the autophagic response is triggered before the apoptotic execution.

Previous evidence has shown that, in certain contexts, the accumulation of autophagosomes or increased levels of LC3B-II can be attributed to a reduced autophagic flux due to a reduced fusion of autophagosomes with lysosomes (to generate autolysosomes) or to a loss of lysosomal digestive function.[43,44] In this case, there would not be a bona fide (i.e., complete) autophagic response characterized by an increased autophagic flux. To ascertain whether the increase in autophagosome formation observed after sorafenib treatment was caused by I) an increase in autophagic activity or II) a reduced turnover of autophagosomes, we arrested the autophagic flux with chloroquine (CQ) and with bafilomycin A_1 (BAF), a lysosomal pH modifier and a vacuolar-type H^+-translocating ATPase inhibitor, respectively, that impair autolysosome formation. Immunofluorescence and quantification of LC3B-II puncta per cell point to an increase in autophagosome formation after sorafenib treatment that was further enhanced when the autophagic flux was arrested with CQ (Figs. 2C and S2H). In addition, we analyzed the levels of SQSTM1; a scaffolding, receptor and cargo protein that is incorporated into newly formed autophagosomes and degraded in autolysosomes. Interestingly, while sorafenib treatment did not result in altered SQSTM1 mRNA levels (Fig. S2I) it enhanced SQSTM1 proteolysis. Accordingly, the addition of CQ and BAF blocked the sorafenib-induced decrease in SQSTM1 levels (Fig. 2D and E), indicating that sorafenib increased the autophagic flux. This was further confirmed by monitoring the autophagic flux by using a chimeric mRFP-GFP tandem fluorescent-tagged LC3B construct (tfLC3).[45] In this assay, and under basal conditions, autophagosomes are observed as a yellow signal (merged mRFP and GFP signal). Under increased autophagic conditions the GFP signal progressively loses fluorescence due to lysosomal acidic and degradative conditions, but mRFP is relatively resistant, thereby labeling autolysosomes in red. Hence, induction of autophagy can be studied by quantifying the increase in both the yellow and red signals. This assay will allow distinguishing between increased autophagic flux and conditions that reduce fusion of autophagosomes with lysosomes, which will typically increase the yellow signal. Our quantification of red (mRFP$^+$ GFP$^-$) and yellow (mRFP$^+$ GFP$^+$) puncta per cell indicates that sorafenib increased the autophagic flux (red and yellow puncta), whereas CQ resulted in the accumulation of yellow puncta (hence autophagosomes). Rapamycin was used as a positive control of increased autophagy flux (Fig. 2F).

Altogether, our results point to a consistent induction of autophagy by sorafenib. These results were complemented by quantification of autophagic structures by transmission electron microscopy (TEM). Our results indicate that sorafenib activated the autophagic flux by increasing the formation of the initial sequestering compartment (the phagophore), the formation of autophagosomes often containing multivesicular and multilamellar structures, and autolysosomes (Figs. 2G and S2J). Finally, because the 3-dimensional (3D) microenvironment can alter autophagy and general intracellular cell signaling when compared with nonpolarized scenarios, we explored sorafenib's capacity to activate autophagy in a setting that more closely recapitulates physiological conditions.[46,47] We assessed sorafenib effects in 3D polarized glandular structures and subcutaneous tumors using Ishikawa and HEC-1A cells, respectively. Organotypic cultures displayed typical cell-to-cell, cell-to-matrix contacts and apical localization of the Golgi apparatus (Fig. S2K). Interestingly, sorafenib was able to activate autophagy in 3D cultures and subcutaneous xenografts, indicating that the sorafenib-induced autophagic response is maintained in 3D polarized glands and subcutaneous tumors (Fig. 2H and I).

Sorafenib-induced macroautophagy is dependent on MAPK8/9/10

Sorafenib induces endoplasmic reticulum (ER) stress, which can restore cell homeostasis or trigger cell death by simultaneously activating multiple interconnected processes such as the unfolded protein response (UPR), hypoxia or, most importantly, autophagy.[28,48,49] Based on this we hypothesized that, in our model, an ER stress response may precede the induction of autophagy by sorafenib. Our results by TEM suggest that sorafenib may induce ER stress, as dilated ER lumens were

Figure 2. (see previous page) Sorafenib treatment activates an autophagic flux. (A) Pearson's correlation coefficients (Y-axis) between gene expression and sorafenib sensitivity of 20 EC cell lines are plotted as a function of the ranking of the coefficients (X-axis). Each data point represents a gene. Gene set enrichment analysis[22] shows lysosomal genes (red circles) are enriched among those with negative correlation between expression and sorafenib sensitivity. (B) Representative western blot and densitometry quantification from 3 independent experiments showing increased LC3B-II after sorafenib (20μM) treatment of 12 h in Ishikawa, HEC-1A and KLE $_{EC}$ cells. Western blot against tubulin was performed to ensure equal protein loading amounts. (C) 12-h sorafenib treatment causes an increase in immunofluorescent LC3B-II puncta per cell that is further increased when sorafenib is combined with CQ, reflecting an autophagic response in Ishikawa and HEC-1A $_{EC}$ cells. Left, representative immunofluorescent images of Ishiwaka cells. Scale bar: 50 μm. Right, quantifications are represented as percentage of total cell population. Statistical values (t-test) compare the number of LC3B-II puncta per cell between conditions. Autophagic flux arrest using 2 different concentrations of CQ (D) and bafilomycin A_1 (E). Ishikawa cells were lysed after 24 h of treatment and levels of SQSTM1 were analyzed by western blot. Western blot against tubulin was performed to ensure equal protein loading amounts. Densitometry quantifications of SQSTM1 from 3 independent experiments are also shown. (F) Autophagic flux analysis. Left, representative immunofluorescent images of Ishiwaka cells transfected with a chimeric mRFP-GFP-LC3B probe showing mRFP, GFP and merged mRFP and GFP (yellow) puncta. Scale bar: 15 μm. Right, quantification of red (mRFP$^+$ GFP$^-$) and yellow (mRFP$^+$ GFP$^+$) puncta per cell. (G) Left, schematic illustration of autophagic process with the most relevant autophagic structures. Right, representative transmission electron microscopy (TEM) images showing formation of phagophores (P), autophagosomes (AP) and autolysosomes (AL) after sorafenib (20μM) treatment of 24 h. Also, quantification of increased P, AP and AL. 100 cells in each condition were quantified using this method (n = 3). Asterisks indicate vacuolization and dilated ER cisternae. N, nucleus. (H) Left, representative micrographs of 3D cultures treated with sorafenib showing decreased cytoplasmic content and the presence of autophagic organelles. Ishikawa cells were cultured in matrigel to form 3D organotypic structures. 3D cultures were left untreated or treated with sorafenib (20μM) for 24 h and subsequently processed for TEM analysis. M, mitochondria. Right, 3D cultures were additionally processed for western blot against LC3B-II. LC3B-II densitometry quantification from 3 independent experiments are also shown. (I) Left, TEM representative micrographs illustrating autophagy activation in response to sorafenib in vivo in HEC-1A subcutaneous tumors injected in SCID mice. Images show a drastic depletion of cytoplasmic subcellular compartments and the presence of autophagic structures. L, lipid droplet. RER, rough endoplasmic reticulum. Xenografts were left to grow for 11 d and mice were injected intraperitoneally with sorafenib 15 mg/kg/d. At the end of the treatment, tumors were collected and processed for TEM. Right, tissue immunohistochemistry for LC3B (dilution 1:100) and SQSTM1 (dilution 1:3000). All experiments were performed in triplicate.
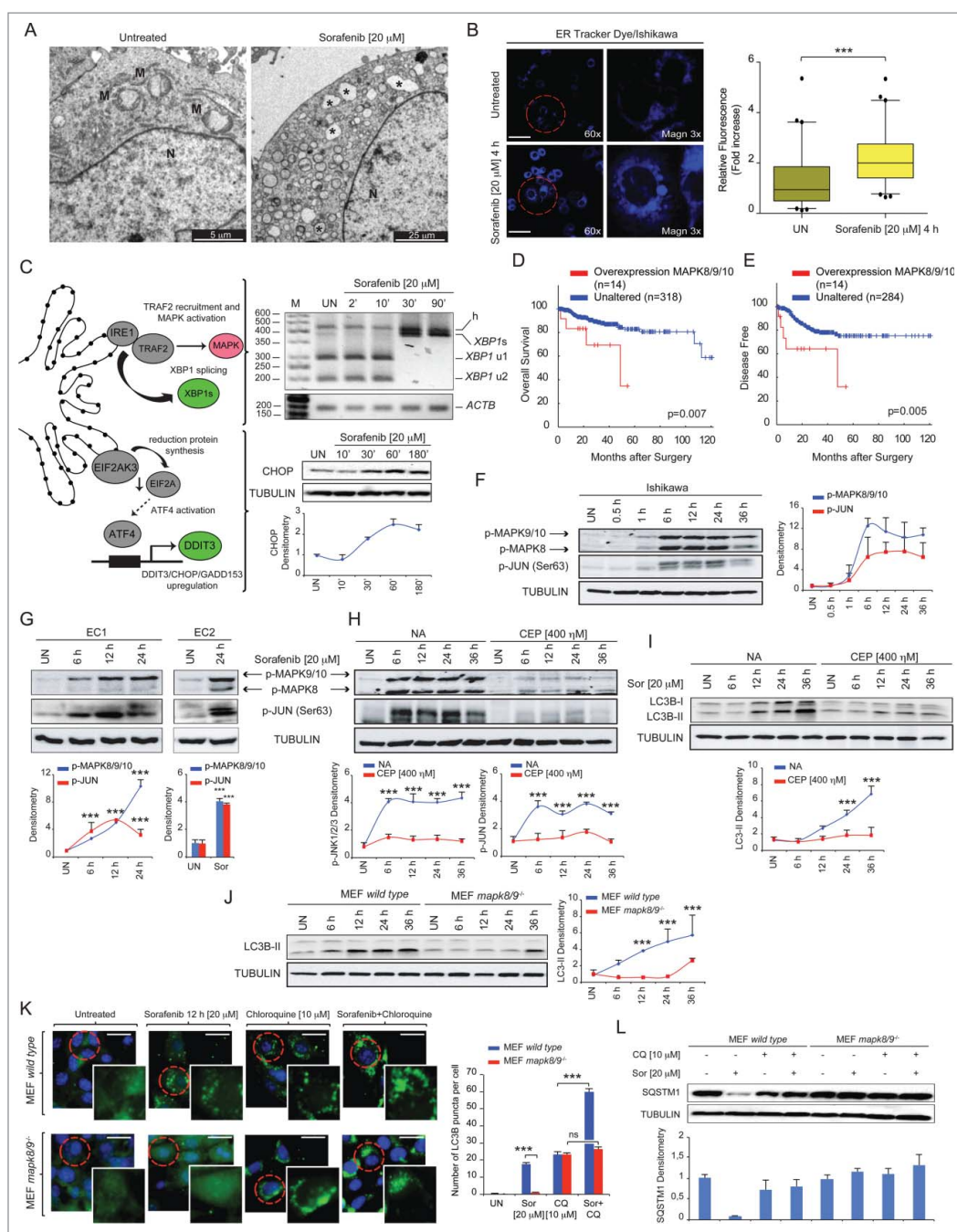
Figure 3. Sorafenib induces autophagy through ER stress and MAPK8/9/10 activation. (A) TEM representative micrographs showing dilated ER cavities in sorafenib-treated Ishikawa cells for 24 h. For additional information please see Fig. S4A. (B) Left, representative images showing increased and discontinuous fluorescence intensity in endoplasmic reticulum upon sorafenib treatment. Untreated and sorafenib-treated Ishikawa cells were cultured in the presence of ER-Tracker Blue-White DPX and analyzed at 4 h post-treatment. Scale bar: 50 μm. Right, quantification of ER-Tracker Blue-White DPX intensity according to refs. [94,95] and using ImageJ software. (C) Left, schematic illustration representing 2 characteristic UPR responses, EIF2AK3/PERK-ATF4 and ERN1/IRE1. Right, *XBP1* splicing analysis by PCR and enzymatic restriction and DDIT3/CHOP protein levels by western blot with densitometry quantification in Ishikawa cells treated with sorafenib. Splicing of *XBP1* mRNA results in the excision of a 26-nucleotide intronic region, causing a frame shift in the coding sequence and the removal of a PstI restriction site. Therefore, PstI can digest unspliced *XBP1* mRNA (*XBP1u*), generating *XBP1 u1* and *u2* fragments, but not spliced *XBP1* mRNA (*XBP1s*). h represents a hybrid band composed of *XBP1u* and *XBP1s* single-stranded DNA produced during PCR. (D) Kaplan-Meyer and (E) disease-free survival curves comparing the outcome of EC cases with or without overexpression of MAPK8/JNK1, MAPK9/JNK2 and MAPK10/JNK3. A z-score≥ 3 was used as threshold for increased expression. Data were extracted from TCGA_ucec (RNAseq_V2). (F) Western blot and densitometry quantification (n = 3) showing activation of MAPK8/9/10 and its target JUN after a time course treatment of sorafenib (20 μM) in Ishikawa cells. (G) Activation of MAPK8/9/10 and JUN by western blot in sorafenib-treated primary EC biopsies. CEP-1347 inhibits activation of MAPK8/9/10 and JUN (H) and blocks LC3B-II increase in Ishikawa EC cells (I). Densitometry quantifications from 3 independent experiments are also shown. (J) Representative western blot and densitometry quantification (n = 3) showing impaired LC3B-II accumulation in *mapk8/9−/−* cells after sorafenib treatment. (K) Representative immunofluorescence images and quantification of the number of LC3B-II puncta per cell in wild-type and *mapk8/9−/−* MEFs treated with sorafenib or sorafenib combined with CQ. Scale bar: 50 μm. (L) Analysis of SQSTM1 protein levels by western blot in wild type and *mapk8/9−/−* MEFs showing that CQ and *Mapk8/9*-targeted deletion abrogates SQSTM1 proteolysis in response to sorafenib in wild-type and *mapk8/9−/−* MEFs. Western blot against tubulin was performed to ensure equal protein loading amounts. SQSTM1 densitometry analysis is also shown. All experiments were performed in triplicate.

frequently observed after treatment (Figs. 2G, 3A, and S3A).[28,48] To test whether this was the case we stained the ER of EC cells with ER-Tracker, a specific ER-fluorescent dye commonly used to indirectly report ER stress.[50-52] Staining of untreated cells revealed the typical reticular cytoplasmic structure while sorafenib-treated EC cells displayed an increased and discontinuous ER intensity (Figs. 3B and S3B). Elevated ER intensity after treatment occurred before autophagy and apoptosis induction, suggesting that ER stress could precede these responses. This was further characterized by analyzing molecular ER stress markers of the UPR such as XBP1 mRNA splicing and the expression of DDIT3/CHOP. Unspliced XBP1 mRNA (XBP1u) harbors 2 open reading frames (ORF1 and ORF2) encoding 2 bZIP proteins of 261 amino acids (aa) and 222 aa, respectively. Upon activation of ER stress, ERN1/IRE1 removes a 26-nucleotide intron, containing a PstI restriction site, from the XBP1 mRNA generating a spliced XBP1 mRNA (XBP1s) encompassing an open reading frame shift that results in the production of a potent 376 aa transcription factor. Since PstI only cuts XBP1u, generating XBP1 u1 and u2 fragments, it is possible to assess XBP1 mRNA splicing by enzymatic restriction. Our data indicate that as soon as 30 min after sorafenib treatment the UPR response was activated as measured by XBP1 splicing and increased DDIT3 protein levels (Fig. 3C) thus confirming our hypothesis.

ER stress has been linked to autophagy induction in part through MAPK/JNK, a critical effector of ERN1 signaling.[53-55] Importantly, MAPK/JNK has been used to predict poor sorafenib response and increased risk of recurrence in hepatocellular carcinoma (HCC) patients.[56] Thus, we resolved to investigate the clinical relevance of MAPK/JNK in EC patients and to dissect its role in sorafenib-induced autophagy. Analysis of survival/recurrence of clinical parameters in EC patients indicated that increased expression of MAPK8/JNK1, MAPK9/JNK2 and MAPK10/JNK3 was associated with poor survival and increased recurrence rates (Fig. 3D and E). Intriguingly, by using an antibody that recognizes phosphorylation of MAPK/JNK at residues Thr183/Tyr185, we observed a consistent activation of MAPK/JNK and the target JUN after sorafenib treatment in EC cell lines and primary EC biopsies. Particularly, their phosphorylated status reached its peak at 6 h and these proteins remained phosphorylated even 36 h after treatment (Figs. 3F, G and S3C). Notably, inhibition of cell death by increased expression of BCL2L1 and MCL1 abrogated sorafenib-induced apoptosis (Fig. S3D and S3E), but could not prevent activation of MAPK/JNK and JUN (Fig. S3F and S3G), indicating that their activation was independent of the apoptotic execution.[30]

Finally, to test whether MAPK/JNK activation plays an instrumental role in the autophagic induction in response to sorafenib we inhibited their activity with CEP-1347, a selective inhibitor of the upstream mixed lineage kinase family that does not block activity of other related kinases such as MAPK/ERK or MAPK/p38 (Fig. 3H).[57,58] Remarkably, addition of CEP-1347 impaired the increase of LC3B-II after sorafenib treatment in EC cells (Fig. 3I). To rule out off-target effects of CEP-1347, we sought to determine the role of MAPK8/9 in wild-type and mapk8/9$^{-/-}$ mouse embryonic fibroblasts (MEFs) treated with sorafenib. As shown in Figs. 3J and S3H, targeted deletion of

Mapk8/9 in MEFs completely abrogated MAPK8/9 and JUN activation in response to sorafenib and significantly delayed LC3B-II accumulation. Analysis of the autophagic flux by quantification of immunofluorescent LC3B-II puncta per cell (Fig. 3K) and analysis of Sqstm1 mRNA/protein levels (Figs. 3L and S3I) in wild-type and mapk8/9$^{-/-}$ MEFs treated with sorafenib or sorafenib plus CQ indicated that MAPK8/9 played an essential role in the autophagic process. Altogether these results indicate that sorafenib induces a UPR response in EC cells that connects with an autophagic output through a MAPK/JNK-dependent mechanism.

Autophagy inhibition potentiates sorafenib lethality in vivo

Sorafenib-induced autophagy can promote resistance or trigger cell death.[33,38-42] On the basis of these lines of evidence, we resolved to dissect its role by inhibiting autophagy in sorafenib-treated cells. To this end we treated EC cells with sorafenib in conditions of autophagy inhibition by using CQ. In addition, we further complemented these data by knocking down BECN1/Beclin 1 expression using small interfering RNA. BECN1, the mammalian ortholog of yeast Vps30/Atg6, is an important regulator of autophagy that is essential for autophagic vesicle nucleation by interacting with the PIK3C3/VPS34 complex and BCL2 homologs.[59] Most importantly, BECN1 has been described as a prognosis factor of poor outcome in endometrial adenocarcinomas.[60] By performing cell viability and apoptosis assays such as ANXA5/annexin-V stainings, quantification of picnotic nuclei and western blot against active caspases, our in vitro data showed that autophagy inhibition with CQ and BECN1 shRNA sensitized EC cells to sorafenib (Fig. 4A-E and S4A), suggesting that autophagy could be a counterbalancing mechanism and an adaptive response to stress.

Next, we aimed to reproduce these results in vivo by testing sorafenib-CQ combination in HEC-1A subcutaneous tumors. Interestingly, after 2 wk of treatment we found that combination of sorafenib with CQ led to a marked reduction in tumor growth (p < 0.001) with the concomitant decrease in SQSTM1 and increase in LC3B protein levels when compared with sorafenib alone (Fig. 4F). We also investigated the ability of sorafenib-CQ to affect lung EC metastatic growth. Metastasis is the main cause of death in patients with cancer and a critical challenge in cancer therapeutics. In fact, autophagy represents an adaptive mechanism during distant tissue colonization, but to date no reports have evaluated the effects of autophagy inhibition in developing EC metastases.[61] By retro-orbitally injecting GFP/luciferase-MFE-296 EC cells into SCID (severe combined immunodeficiency) mice, we engineered a lung-EC metastatic model. Strikingly, while metastases in control, CQ- and sorafenib-treated mice grew unopposed, combined sorafenib-CQ treatment significantly delayed metastatic growth and resulted in increased survival rates (Fig. 4G and H). Subsequent histological analyses and quantification of metastases sizes revealed necrotized areas and reduced diameter of metastases (Fig. 4I and J). These results indicate that autophagy could represent a cytoprotective mechanism that can potentially be explored therapeutically in EC.

Autophagy inhibition potentiates sorafenib effects in orthoxenograft models and plays a role in EC progression/recurrence

In recent years autophagy has received increasing attention in gynecological malignancies, but its function and therapeutic value is still uncertain.[60,62-65] Because the use of conventional cell lines lacks predictive value in terms of drug development or clinical testing, we set up a platform to perform sorafenib translational studies using primary EC-derived orthoxenografts.[66] Orthoxenograft models present the advantage of their high predictive drug-response value and their accuracy recapitulating the main features of donor tumors including tissue morphology (Fig. S5A).[67] Grade 1-to-3 primary EC samples
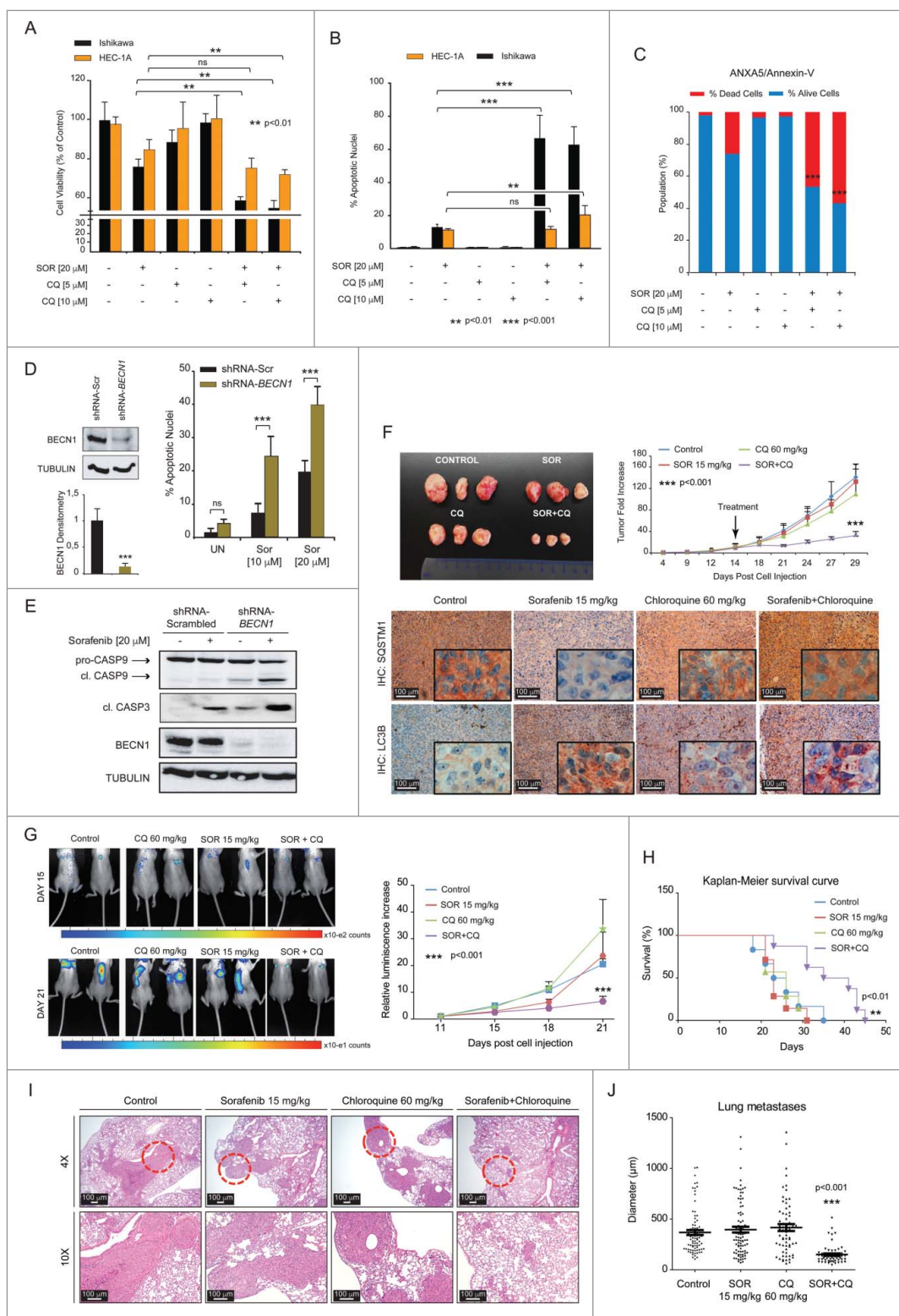

Figure 4. (For figure legend, see page 616)

were collected, orthotopically implanted in recipient female mice and the potentiating effects of CQ were assessed using suboptimal doses of sorafenib (Fig. 5A). Our analyses indicate that sorafenib-CQ markedly impaired tumorigenesis when compared with either condition alone (Figs. 5B-D and S5A) without causing systemic toxicity (Fig. S5B). Altogether these results indicate that autophagy inhibition using CQ potentiates sorafenib effects in patient-derived tumor orthoxenografts and provide insights into the modest effects of sorafenib trials in EC patients.

Discussion

In this study we have shed light on the mechanisms behind sorafenib inefficacy to improve the outcome of advanced and recurrent uterine carcinoma and carcinosarcoma patients.[20] Sorafenib is currently being administered in patients with advanced renal cell carcinoma, hepatocellular carcinoma and most recently in metastatic thyroid carcinoma where it has been shown to improve patient overall survival.[13,14,68] Unfortunately, most patients develop disease progression and increasing efforts are dedicated to understand sorafenib resistance at a mechanistic level.[69,70] Initial findings indicate that acquisition of sorafenib resistance could involve the activation of compensatory mechanisms.[71] Using bioinformatics analysis and our in vitro/in vivo experimental data, we have unraveled autophagy as a molecular pathway underpinning this resistance in EC. The induction of a protective autophagic response by sorafenib has been described previously, but this is the first study reporting this phenomenon in EC and using patient-derived tumor orthoxenotransplants.[38,72,73] Autophagy is a biologically highly conserved and regulated catabolic process that recycles macromolecules, long-lived proteins and organelles through their inclusion within double-membrane-bound structures (autophagosomes) and subsequent fusion with lysosomes (to generate autolysosomes). Here, cargo elements will be hydrolyzed into basic biomolecules, recycled back to the cytosol and reutilized by anabolic pathways to build new proteins and organelles.[74] Recently, autophagy has been shown to be regulated in normal endometrium across the menstrual cycle and to play a relevant role in ovarian endometriosis.[75-77] However, the contribution of autophagy and its therapeutic potential in the development and progression of EC is still underexplored.

By using an array of techniques, our data indicate that sorafenib is able to induce a MAPK/JNK-dependent autophagic response in EC cells that has its origin early during ER stress. Interestingly, MAPK/JNK can execute autophagy by regulating the interaction between BECN1 and several members of the BCL2 family and this could explain why increased MAPK/JNK activity has been proposed as a predictive biomarker for poor sorafenib response and increased risk of recurrences in HCC patients.[56,78,79] Similarly, increased MAPK8/JNK1, MAPK9/JNK2 and MAPK10/JNK3 expression correlates with poor prognosis in EC patients, suggesting that MAPK/JNK may play an unforeseen key function favoring EC progression/recurrence. Nonetheless, their characterization as instrumental factors driving EC relapse is still uncertain and warrants additional investigations.

The role of autophagy during tumor progression and response to stress is largely unclear and dissecting its biological function has been demonstrated to be challenging, presumably because of its context-dependent biology.[80] For instance, autophagy is thought to exert tumor suppressor properties in the initial steps during tumorigenesis by inhibiting necrosis and consequent immune cell infiltration within the primary tumor. Conversely, autophagy can endow cells the ability to adapt and to thrive within new hostile environments by protecting cancer cells from undesired threats at late tumor stages (e.g., vascular intravasation, extravasation and colonization at distant sites).[80] Most importantly, some cancer cells possess the ability to hijack and tweak the adaptation cues triggered by autophagy to cope with the stress induced by anticancer treatments.[33,37-39,81] Therefore it is not surprising that, in certain conditions, autophagy inhibition has been demonstrated to potentiate re-sensitization to anticancer therapy.[81-85] We reasoned that this could be the case for sorafenib in the context of EC. By inhibiting autophagy with CQ and BAF our in vitro/in vivo experiments using cell lines and orthotopic EC patient-derived xenotransplants demonstrate that autophagy may act as a protective mechanism against sorafenib. Remarkably, this is the first report using primary EC orthoxenografts that addresses autophagy inhibition as a complementary therapy to sorafenib in cancer samples.

Figure 4. (see previous page) Autophagy inhibition potentiates sorafenib anticancer properties. (A) MTT cell viability assay in sorafenib (SOR)-treated Ishikawa and HEC-1A cells in combination with chloroquine (CQ) for 12 h. Values are represented as the percentage of viable cells compared with untreated cells. (B) Quantification of percentage of pyknotic nuclei by Hoechst staining of Ishikawa and HEC-1A cells treated with sorafenib in combination with CQ for 12 h. (C) Analysis of ANXA5/Annexin V-positive Ishikawa cells by flow cytometry after sorafenib treatment combined with CQ for 12 h. Values are expressed as percentage of cells in relation to total number of cells. (D) Left, western blot and densitometry quantification (n = 3) showing decreased BECN1 expression in *BECN1*-shRNA infected Ishikawa (IK) cells. Western blot against tubulin was performed to ensure equal protein loading amounts. Ishikawa cells transduced with lentiviral particles encoding shRNA-scrambled or shRNA-*BECN1* and selected with puromycin. Right, quantification of apoptotic nuclei after 2 doses of Sorafenib treatment of 24 h in shRNA-scrambled Ishikawa cells and cells with constitutive decreased expression of *BECN1*. (E) Western blot showing increased activation of inducer CASP9 and executioner CASP3 in shRNA-*BECN1* Ishikawa cells after sorafenib (20 μM) treatment of 24 h. (F) HEC-1A subcutaneous tumors. Fourteen d after HEC-1A injection, mice were randomized and treated with vehicle (n = 5), CQ 60 mg/kg (n = 5), sorafenib 15 mg/kg (n = 5) and sorafenib plus CQ (n = 5) and processed at d 29. Top-left, representative image of subcutaneous tumors after treatment. Top-right, subcutaneous tumor growth kinetics. No differences in tumor size were noticed between vehicle and CQ (1.41 $\pm$ 0.21cm,^{3} 0.90 $\pm$ 0.08cm^3; p = 0.221), when comparing vehicle with sorafenib (1.41 $\pm$ 0.21cm,^{3} 1.15 $\pm$ 0.19cm^3; p = 0.161) or between CQ and sorafenib (0.90 $\pm$ 0.08cm,^{3} 1.15 $\pm$ 0.19cm^3; p = 0.447). Notably, combination of sorafenib with CQ (0.25 $\pm$ 0.04cm^3) led to a marked reduction in tumor volume in all mice (p < 0.001) when compared with either agent alone. Values are represented as tumor volume fold increase in relation to d 4 after injection. Down, tissue immunohistochemistry for LC3B (dilution 1:100) and SQSTM1 (dilution 1:3000). All experiments were performed in triplicate. (G) Inhibition of metastatic EC growth by sorafenib combined with CQ. EC cells MFE-296 were stably infected with EGFP-luciferase. After selection, 50×10^4 MFE-296 cells were retro-orbitally injected and 11 d after injection mice were treated with vehicle (n = 5), CQ 60 mg/kg (n = 5), sorafenib 15 mg/kg (n = 5) and sorafenib plus CQ (n = 5) until d 21 (see Materials and Methods for further details). Left, representative bioluminescence imaging comparing progression of metastasis in lungs at 15 and 21 d after injection of MFE-296 cells. Right, quantification of the relative bioluminescence intensity. Values are expressed as fold increase in relative luciferase units (RLU) compared with time 0 (11 d post-injection). (H) Kaplan-Meyer survival curve of mice retro-orbitally injected with MFE-296 cells and treated until d 21. At d 21, treatment was terminated and mice were monitored twice a day. (I) Representative lung morphology analysis by hematoxylin and eosin staining. Samples were harvested at d 21 based on bioluminescent and survival analysis (n = 5/condition). (J) Quantification of metastases diameter.
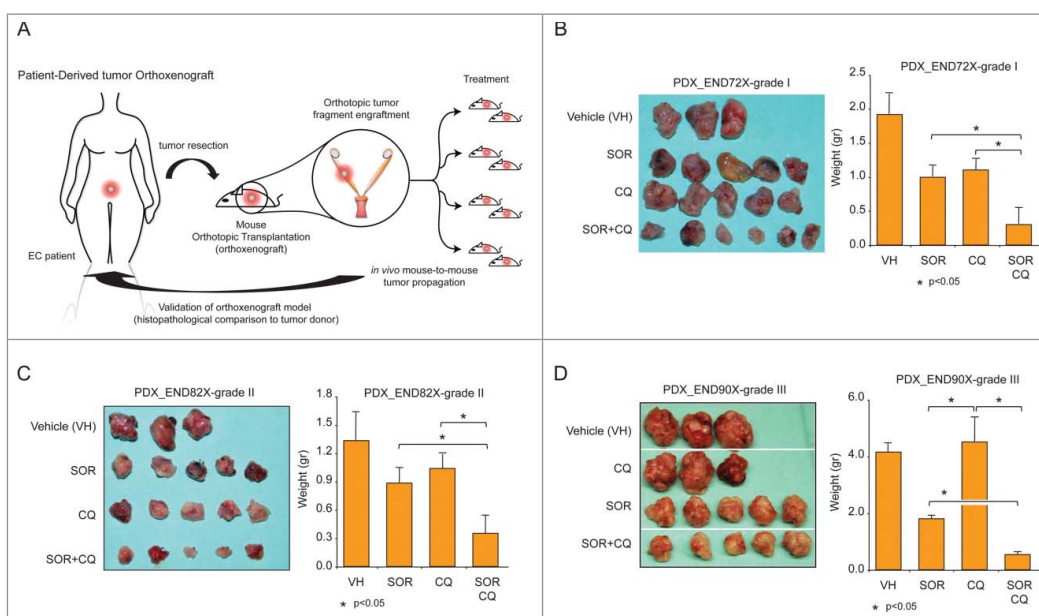
Figure 5. Autophagy inhibition potentiates sorafenib cytotoxicity in orthotopic patient-derived xenotransplants. (A) Schematic representation of patient-derived orthoxeno-transplant implants procedure and treatment. EEC tumors were surgically removed and small pieces were implanted in recipient female mice. Once engrafted, tumors were propagated to a cohort of 20–45 mice, randomized and treated accordingly. Response of engrafted grade-I END72X (B), grade-II END82X (C) and grade-III END90X (D) tumors after control, sorafenib (30 mg/kg), CQ (60 mg/kg) and sorafenib plus CQ treatments. Animals were treated through 21 d (see Materials and Methods). Graphs illustrate responses of 3 endometrial orthoxenografts of different histological degree after 21 d of treatment. Representative images of endometrial-engrafted tumors are also shown.

Patient-derived orthoxenograft and conventional models represent an ideal experimental setting to study drug response treatments. Indeed, several studies point to the high correlation in the response to conventional anticancer treatments between the patient and the concomitant personalized xenograft.[86,87] Moreover, a high predictive drug response has been demonstrated when patient therapeutic decision was based on experimental drug screening using personalized tumor graft models.[88] All these determinants have postulated patient-derived orthoxenografts as an instrumental system in aiding clinical trial limitations and the development of personalized medicine.[67] Altogether, our results indicate that autophagy inhibition could represent a good therapeutic strategy to potentiate sorafenib effects in EC and could explain the resistance to sorafenib observed in advanced or recurred EC patients.

Materials and methods

Reagents and antibodies for western blot

The following reagents were used: chloroquine (Sigma-Aldrich, C6628), rapamycin (Sigma-Aldrich, R0395), 2,5-diphenyl tetrazolium bromide assay (MTT; Sigma-Aldrich, M2128), DMSO (Sigma-Aldrich, W387520), bisbenzimide H33258 (Sigma-Aldrich, B2261), anti-tubulin (Sigma-Aldrich, T8203), anti-DDIT3/CHOP (Sigma-Aldrich, G6916), anti-MCL1 (BD Biosciences, 554103), anti-BCL2L1/BCL-XL (BD Biosciences, 610210), anti-cleaved-CASP9/caspase-9 (Cell Signaling Technology, 9501), anti-cleaved-CASP3/caspase-3 (Cell Signaling Technology, 9661), anti-p-JUN/c-Jun (Ser63) (Cell Signaling Technology, 9261), anti-p-MAPK9/SAPK/JNK (Thr183/Tyr185) (Cell Signaling Technology, 9251), anti-MAPK9/SAPK/JNK (Cell Signaling Technology, 9252), anti-p-EIF4E (Ser209) (Millipore Corporation, 07–823), anti-MAP1LC3B (H-50; Santa Cruz Biotechnology, 28266), anti-BECN1 (Novus Biologicals LLC, NB500–249), anti-SQSTM1/p62 (Novus Biologicals LLC, NBP1–48320), and anti-PARP (Neomarkers/Thermo-Fisher Scientifics Rockford, RB-1680-P0). Sorafenib (BAY54–9085) was obtained from Bayer.

Cell lines and 2D culture conditions

RL95–2, KLE and HEC-1A cells were a gift from Dr. Reventos (Hospital Vall d'Hebron, Barcelona). These cells and the Ishikawa 3-H-12 (Sigma-Aldrich, 99040201) and MFE-296 (Sigma-Aldrich, 98031101) cells were grown in Dulbecco's modified Eagle's medium (DMEM; Sigma-Aldrich, 12007559) supplemented with 10% fetal bovine serum (FBS; Invitrogen, 10270106), 1 mmol/L HEPES (Sigma-Aldrich, H3375), 1 mmol/L sodium pyruvate (Sigma-Aldrich, P2256), 2 mmol/L L-glutamine (Sigma-Aldrich, C59202), 1% penicillin/streptomycin (Sigma-Aldrich, P4333) at 37°C with saturating humidity and 5% CO_2.

For retro-orbital metastatic assay MFE-296 cells were transfected with the luciferase reporter pLKO.Luc (kindly provided by Prof Eloi Garí, Institut de Recerca Biomèdica de Lleida, Catalonia) and selected with puromycin (Sigma-Aldrich, P7255), and maintained in regular medium. All experiments were conducted with low passage cells from recently resuscitated frozen stocks. Cell lines were subjected to comprehensive quality control and authentication procedures, including short tandem repeat profiling for human cell lines, species verification by DNA barcoding, verification of morphology, and testing for fungi, mycoplasma, and other bacteria.

3D spheroid cultures

Growth of endometrial epithelial cells in 3D cultures was performed as described previously with minor modifications.[89]

Briefly, cells were washed with HBSS (Thermo Fisher Scientific, 11520476) and incubated with trypsin-EDTA solution (Sigma-Aldrich, T4049) for 3 min at 37°C. Trypsin activity was stopped by adding DMEM containing 10% fetal bovine serum. Cells were centrifuged at $18 \times g$ for 3 min and diluted in DMEM-F12 medium (Sigma-Aldrich, 11580376) containing 3% Matrigel (BD Biosciences, 354234) and 2% dextran-coated charcoal-stripped serum (HyClone Laboratories, Inc., 11571821), obtaining 1×10^4 cell/mL. Cells were cultured for 4–7 d in an incubator at 37°C with saturating humidity and 5% CO_2. For immunofluorescence, cells were seeded in a volume of $40 \mu L$ per well in 96-well black plates with a microclear bottom (Greiner Bio-One, 655090).

Propidium iodide (PI) staining, ANXA5 apoptosis assay and flow cytometry

Analysis of cell cycle distribution was determined using propidium iodide (PI; Sigma-Aldrich, P4170) staining and flow cytometry. Following treatment, approximately 1×10^6 cells were fixed in 70% ethanol for at least 1 h on ice. Cells were then resuspended in 2 ml of cell cycle buffer (20 μg/ml PI) in phosphate-buffered saline (PBS; Sigma-Aldrich, PBS1), containing 0.1% Triton X-100 (Sigma-Aldrich, T8787) and 50 μg/ml RNase A (Sigma-Aldrich, R5503) for 1 h at 37°C. Apoptosis of human endometrial cells was detected using an ANXA5/annexin V apoptosis assay (Roche Applied Science, 185777) followed by flow cytometry analysis. In brief, cells were harvested following mild trypsinization, washed in PBS, and stained with fluorescein isothiocyanate (FITC)-labeled ANXA5 and PI. The percentage of apoptotic cells was evaluated using FACSCanto II flow cytometer (BD Biosciences, USA), using the following criteria: (i) viable cells: ANXA5-FITC and PI negative, (ii) cells in early apoptosis: ANXA5-FITC positive and PI negative, and (iii) cells in late apoptosis: ANXA5-FITC and PI positive. PI and ANXA5-FITC fluorescence emission was measured with a FACSCanto II flow cytometer (BD Biosciences, USA), and cell cycle distribution was analyzed with WINMDI 2.9 software (The Scripps Research Institute, USA).

XBP1 splicing assay

Total RNA was prepared from the human Ishikawa cell line using Trizol reagent (Invitrogen, 15596026). mRNA was reverse-transcribed (RT) to cDNA (42°C for 1 h, 50°C for 1 h, and 90°C for 10 min) using random hexamers and Superscript II reverse transcriptase (Applied Biosystems, 18064014). Negative control RT-minus reactions were carried out to establish that the target RNA was not contaminated with DNA. The cDNA product was used as a template for subsequent PCR amplifications. The following method was used for detection of spliced and unspliced mRNAs transcribed from the XBP1 gene. Briefly the RT-PCR product of XBP1 mRNA was synthesized primers using primers 5′ GGCCTTGTGGTTGAGAACCAG-GAG 3′ (sense) 5′ GAATGCCCAA AA GGATATCAGACTC 3′ (antisense) with the following PCR protocol: 30 cycles of PCR amplification including initialization at 94°C for 4 min, denaturation at 94°C for 10 sec, annealing at 63°C for 30 sec, elongation at 72°C for 30 sec, and final elongation at 72°C for 10 min. Because a 26-bp fragment contains a PstI site that is spliced upon the activation of XBP1 mRNA, the RT-PCR products were digested with PstI (Takara Bio Inc., 1073A). The housekeeping gene ACTB/β-actin was used as a loading control; primers 5 AGAGCTACGAGCTGCCTGAC' 3′ (sense) and 5′ AGCACTGTGTTGGCGTACAG 3′ (antisense). Subsequent electrophoresis revealed the inactive form as 2 cleaved fragments and the active form as a noncleaved fragment.

Immunofluorescence

2D or 3D cultures were fixed with formalin for 5 min at room temperature, and washed twice with PBS. Depending on primary antibody, cells were permeabilized with 0.2% Triton X-100 in PBS for 10 min or permeabilized with 100% methanol for 2 min. Next, cultures were incubated overnight at 4°C with the indicated dilutions of antibodies: anti-CDH1/E-Cadherin (1:200, Triton X-100; BD Biosciences, 610181); anti-LAM/Laminin (1:500, Triton X-100; Sigma-Aldrich, L9393); anti-GOLGA2/GM130 (1:100, methanol; BD Biosciences, 610822); rhodamine-conjugated phalloidin (1:500, Triton X-100; Sigma-Aldrich, P1951) and anti-MAP1LC3B (1:200, Triton X-100; Cell Signaling Technology, 2775). After 1 day, cells were washed twice with PBS and incubated with PBS containing $5 \mu g$/mL of Hoechst 33342 and a 1:500 dilution of secondary anti-mouse Alexa Fluor 546 (Invitrogen, A11005) and Alexa Fluor 488 (Invitrogen, A11029) or anti-rabbit antibodies Alexa Fluor 594 (Invitrogen, R37119) and Alexa Fluor 488 (Invitrogen, A11034) for 4 h at room temperature. For double-immunofluorescence staining, cells were incubated with the second round of primary and secondary antibodies. In all double-immunofluorescence stains, first and second primary antibodies were from a different isotype. Immunofluorescence staining was visualized and analyzed using confocal microscopy (model FV1000; Olympus, Tokyo, Japan) with the ×10 and the oil-immersion ×60 magnification objectives. Analysis of images was obtained with Fluoview FV100 software (Olympus, Tokyo, Japan).

Subcutaneous tumor xenografts, retro-orbital injections and treatment administration

Flank xenograft tumors: immunodeficient 12-wk-old female SCID hr/hr mice (weight 20–25 g) were maintained in specific pathogen-free (SPF) conditions and manipulated in accordance with institutional guidelines approved by the IRBLLeida regional committee for animal care. Animals were subcutaneously injected with HEC-1A cells (1.5×10^6) suspended in $100 \mu l$ PBS+Matrigel (1:1). Tumors were allowed to grow for 14 d. Mice were randomized and treated with an intraperitoneal injection of chloroquine (60 mg/kg/day) for 2 wk. Sorafenib (BAY 54–9085) was dissolved in a 50% Kolliphor® EL (Sigma-Aldrich, 61791–12–6) 50% absolute ethanol (Scharlau S.L., ET00061000) mixture to a concentration of 60 mg/mL and was administered (15 mg/kg/day) by oral gavage for 2 wk. Tumors were measured 3 times/wk with calipers. Tumor size was calculated as $(D \times d2)/2 = mm^3$.

Retro-orbital metastasis model: 50×10^4 MFE-296 cells expressing EGFP-luciferase were injected retro-orbitally into

the sinus of immunodeficient SCID females. Retro-orbital injections were conducted under 2% isoflurane/air anesthesia. A successful retro-orbital injection was indicated on d 0 by images showing systemic bioluminescence distributed throughout the animals; 6–10 animals/group, with evidence of a satisfactory injection, continued the experiment. Eleven d after injection, when metastases were already noticeable, treatment was initiated as mentioned. Every 3–4 d we monitored tumor lesions by Photon Imager (Biospace Mesures; France) coupled to live imaging software M3 Vision Viewer. For bioluminescence tumor imaging, luciferin (Caliper Life Science, 119222) was used as the substrate for the luciferase expressing tumor cells and injected intraperitonealy at 150 mg/kg in PBS.

Human tissue samples selection and tissue micro arrays (TMAs) construction

Three TMAs were constructed using the manual arrayer from Beecher Instruments Inc., (WI, USA). TMAs contained formalin-fixed, paraffin-embedded tissue of 77 primary endometrioid endometrial carcinomas (ECC) and 24 nonendometrioid endometrial carcinomas (NEEC). A TMA composed of normal endometrium (24 cases) in different phases of the menstrual cycle was also included (18 proliferative, 6 secretory). The tumors were classified following the most recent WHO criteria. They were surgically staged and graded according to the International Federation of Gynecology and Obstetrics (FIGO) staging and grading systems. They included 19 grade 1 EECs, 28 grade 2 EECs, and 30 grade 3 EECs. Samples were obtained from the surgical pathology files of Hospital Universitari Arnau de Vilanova, Lleida, Spain (HUAV). The local ethics committee approved the study and informed consent was obtained from each patient. All tissue samples were histologically reviewed and representative tumor or nontumor areas were marked in the corresponding paraffin blocks. Tissue cylinders with a diameter of 0.6-mm were punched from 2 different tumor areas of each "donor" tissue block and brought into a recipient paraffin block.

TMA immunohistochemistry

TMA blocks were sectioned at a thickness of 3 μm, dried for 1 h at 65° before the pre-treatment procedure of deparaffinization, rehydration and epitope retrieval in the Pre-Treatment Module, PT-LINK (DAKO) at 95°C for 20 min in 50x Tris-EDTA buffer (DAKO, K8002), pH 9. Before staining the sections, endogenous peroxidase was blocked. The antibodies used were anti-MAP1LC3B (1:100 dilution) and anti-p62/SQSTM1 (1:100 dilution). After incubation, the reaction was visualized with the EnVisionTM FLEX Detection Kit (DAKO, K8024) using diaminobenzidine chromogen as a substrate. Sections were counterstained with hematoxylin. Appropriate negative controls including no primary antibody were also tested. The immunohistochemistry was evaluated semi-quantitatively by the intensity and the presence or not of punctate staining. To exclude subjectivity, 2 members of the team evaluated all slides independently. A histological score was obtained from each sample, which ranged from 0 (no punctate staining) to 3 (maximum immunoreactivity). Since each TMA included 2 different

tumor cylinders from each case, immunohistochemical evaluation was done after examining both samples.

Analysis of TCGA data

Normalized gene expression data (RNA-Seq z-score) were downloaded from cBio portal, including 5254 genes and 373 samples.[90,91] Each z-score value represents the gene expression of a sample compared with tumors that have 2 copies of the gene. Clinical information (overall survival and disease-free progression) was obtained from. ref. 5. Survival analysis was performed using Kaplan-Meier estimator and log-rank test. RNA z-score$\geq$ 3 was used to define overexpression of a gene to help stratify patients in survival analysis. To test for differential survival due to potential MAPK/JNK activities, we stratified patients according to overexpression of MAPK8/JNK1, MAPK9/JNK2 or MAPK10/JNK3.

Analysis of drug sensitivity data

We obtained the cell-line sensitivity to kinase inhibitors from McDermott et al.[21] We focused our analysis on the 12 drugs with sensitivity data for uterus cell lines. The total number of cell lines with the sensitivity data are between 493 and 500, depending on the drugs. To test if uterus cell lines are sensitive to a drug, GSEA was applied.[22] For each drug, we ranked cell lines according to their sensitivity and test if uterus cell lines are over-represented among sensitive cell lines. We used 1000 permutations to assess the significance of enrichment. In addition, a t test was used to test if uterus cell lines (n = 7) have differential sensitivity compared with all other cell lines (n = 487).

Additionally, we obtained the gene expression (microarray) and drug sensitivity data of cell lines derived from endometrium (n = 20) from Barretina et al.[34] Gene expression data were processed with the MAS5 algorithm.[92] Probes hybridized to multiple genes were discarded. The data were log2 transformed and probes with low ($<$ 6, log2 scale) or high ($>$ 15.5) values in $>$20% of the samples were discarded. Data were normalized according to the 75th percentile of each sample. Gene-level expression was obtained by averaging values of probes hybridized to the same gene. Genes with low variance (SD $<$ 0.7) were discarded. We then calculated Pearson's correlation coefficients between the expression of each gene (6578 genes after the above filtration) and the sensitivity to sorafenib (activity area).[34] GSEA was used to identify biological processes (Gene Ontology)[93] that are enriched for genes whose expression are positively or negatively correlated with sensitivity to sorafenib (1000 permutations).

Generation of orthoxenografts® of endometrial carcinomas in mice

Three endometrial orthoxenografts (endometrioid carcinomas from different histological degree) were selected from a previously established library of 75 endometrial orthoxenografts (ENDX) developed in nude mice after ortothopic implantation of small pieces of primary human fresh surgical specimens (A. Vidal and A. Villanueva, unpublished data). To generate the library, the tumors were obtained at Hospital Universitari de

Bellvitge (L'Hospitalet de Llobregat, Barcelona,Spain) between 2010 and 2015. Nonnecrotic tissue fragments (ca. 2-3 mm^3) from resected tumors were selected and placed in DMEM medium supplemented with 10% FBS and penicillin/streptomycin at room temperature. Under isofluorane-induced anesthesia, animals (n = 2 to 4) were subjected to a lateral laparotomy, their uterus exposed and tumor pieces anchored with prolene 7.0 sutures, and the abdominal incision was closed with surgery staples. Tumor growth was monitored twice per wk and when the tumor grew, it was harvested, cut into small fragments, and transplanted into 2 to 4 new animals. Engrafted tumors at early mouse passages (#1 to #3) were cut in 6- to 8-mm^3 pieces and stored in liquid nitrogen in a FBS-based solution and 10% dimethyl sulfoxide for subsequent implantation.

Three endometrial orthoxenografts (grade-I ENDX72, grade-II ENDX80, grade-III ENDX90) were selected from the library, and they were defrosted, washed several times in DMEM medium supplemented with 10% FCS and penicillin/streptomycin, and newly re-implanted in the uterus of 3 young nude mice. After an elapsed time of 2–3 mo, tumors grew as orthotopic implants in nude mice, and they were passed to 5 animals (pre-experiment). Animals were housed in a sterile environment, cages and water were autoclaved, and bedding and food were γ-ray sterilized. A good histology correlation was seen between primary and xenografted tumors, as along different mouse-to-mouse passages. None of the endometrial cancer patients had received previous cytotoxic chemotherapy treatment. All patients gave written consent to participate in the study and the Ethics Committee of hospitals cleared the study protocol; animal experimental design was approved by the IDIBELL animal facility committee.

Drug response assay in endometrial orthoxenografts

For each tumor, small fragments of 2–5 mm^3 of xenografted tumors obtained in the previous pre-experiment were re-implanted in one of the arms of the uterus of 30 female nude mice as described above. When tumors reached a homogeneous palpable size (10 d for ENDX90; 35 d for ENDX82; and 52 d for ENDX72) they were randomly allocated into the treatment groups (n = 5–9/group): i) placebo; ii) sorafenib (30 mg/kg); iii) chloroquine (60 mg/kg); and iv) sorafenib plus chloroquine (30+60 mg/kg). Animals were treated daily during 21 d with chloroquine (administered 1 h before by intraperitoneal injection), whereas for sorafenib (oral gave) we followed a schedule of 2 d ON, 1 OFF to reduce drug-induced toxicity. At d 23, animals were killed, their uterus dissected out, and tumors weighed and measured with a caliper. Representative fragments were either frozen in nitrogen or fixed and then processed for paraffin embedding. Additionally, the lungs, liver and diaphragm tissues were taken for histological study of the presence of metastases.

Statistical analysis in vivo experiments

Values are presented in the graphs as the mean ± standard errors of the mean (SEM) of n cell-based experiments or n biopsies where each value is the average of responses in triplicate, at least. Statistical analysis was performed with GraphPad Prism 6.0. Differences between 2 groups were assessed by the Student t test. Differences between more than 2 groups were assessed by ANOVA, followed by the Tukey's multiple comparison test. $p < 0.05^*$, $p < 0.01^{**}$ and $p < 0.001^{***}$ were considered statistically significant.

Transmission electron microscopy

Cut samples (roughly 2 mm^3) were immersed in 2.5% glutaraldehyde, 0.1 M PBS, pH 7.4 for 12 h at 40°C, postfixed for 2 h in 1% osmium tetroxide, dehydrated in acetonitrile and embedded with Embed-812 epoxy resin (Electron Microscopy Sciences, 14120). Ultrathin sections of 80 nm were counterstained with uranyl acetate and lead citrate and observed in a Zeiss EM 910 (Zeiss) electron microscope.

Clonogenicity assay

Cells were seeded onto 6-well plates at a density of 1×10^3 cells per dish. Twenty-four h later, cells were treated for the indicated hours after which the medium was changed and cells incubated at 37°C in 5% CO$_2$ for 15 d. Colonies were stained with 0.4 mg/mL MTT final concentration for 30 min, fixed in 100% methanol (VWR International, 1060092500) for 5 min and maintained in 2 mL PBS. Colonies consisting of > 50 cells were scored using the Quantity One software (Bio-Rad Laboratories, USA).

Total RNA extraction, reverse transcriptase-polymerase reaction (RT-PCR) and quantitative real-time qRT-PCR

Total RNA was extracted from the indicated cell lines using the RNeasy Total RNA kit (Qiagen, 74104). mRNA was reverse-transcribed (RT) to cDNA (42°C for 1 h, 50°C for 1 h, and 90°C for 10 min) using the High Capacity cDNA Archive Kit (Applied Biosystems, 4368813). Negative control RT-minus reactions were carried out to establish that the target RNA was not contaminated with DNA. The cDNA product was used as a template for subsequent PCRTaqman® technology from Applied Biosystems was used for real-time qRT-PCR analyses. Human Probes: GAPDH, Hs99999905_m1; p62/SQSTM1, Hs00177654_m1. Mouse Probes: Gapdh, Mm99999915_g1; p62/sqstm1, Mm00448091_m1. For qRT-PCR assay the cDNA was amplified by heating to 95°C for 10 min, followed by 40 PCR cycles of 95°C for 15 sec and 60°C for 1 min using GoTaq® qPCR Master Mix (Promega Corporation, A6001) and ABI Prism 7900 Sequence Detection System (Applied Biosystems, USA). Relative mRNA expression levels were calculated using the 2ΔΔCt method and are presented as ratios to the housekeeping gene GAPDH. Each sample pool was amplified in triplicate using GAPDH for normalization.

ER stress analysis

Cells were incubated with diluted 1:1000 ER-Tracker Blue-White DPX (Molecular Probes, E12353) in DMEM medium. Pre-warmed (37°C) probe-containing medium was added to the cells and incubated for 30 min. Thereafter, loading solution

was removed and cells were washed with PBS before adding fresh medium without probe. Cells were analyzed using a fluorescence microscope and a confocal laser scanning microscope model FV1000-Olympus, at ×10 and ×60 magnification objectives. Analyses of images were obtained with Fluoview_FV100 software. We have quantified the intensity of ER staining as previously performed using the ImageJ software.[94,95]

mRFP-GFP tandem fluorescent-tagged LC3B (tfLC3) autophagic flux assay

Ishikawa cells were transfected with tfLC3 plasmid (kindly provided by Dr. Tamotsu Yoshimori, Osaka University, Japan[45]) and left to grow overnight before treatment with sorafenib (20 μM), chloroquine (10 μM) and rapamycin (500 nM) during 12 h. After this period, cell were fixed with paraformaldehyde solution (4% in PBS), washed twice with PBS and analyzed with a confocal laser scanning microscope (Olympus, FV1000). Images were acquired randomly and cells displaying intermediate total mRFP-GFP fluorescence were chosen for analysis. Each channel was acquired by a separate scan avoiding bleedthrough. We analyzed all cells using the same threshold settings across all images from each channel. Double mRFP-GFP puncta were determined using the Colocalization plugin in ImageJ. All puncta were quantified using the Analyze Particle plugin in ImageJ.

Dedication

This work is dedicated to Lluc and Gemma.

Abbreviations

3D	3-dimensional
ANXA5	annexin A5
BAF	bafilomycin A$_1$
BCL2	BCL2, apoptosis regulator
BCL2L1/BCL-XL	BCL2 like 1
BECN1/ATG6	Beclin 1
CQ	chloroquine
DDIT3/CHOP DNA	damage inducible transcript 3
EC	endometrial cancer
EIF4E	eukaryotic translation initiation factor 4E
ER	endoplasmic reticulum
ERN1/IRE1	endoplasmic reticulum to nucleus signaling 1
GFP	green fluorescent protein
GSEA	gene set enrichment analysis
IK	ishikawa cell line
MAP1LC3B	microtubule-associated protein 1 light chain 3 β
MAPK8/JNK1	mitogen-activated protein kinase 8
MAPK9/JNK2	mitogen-activated protein kinase 9
MAPK10/JNK3	mitogen-activated protein kinase 10
MCL1 BCL2	family apoptosis regulator
MEF	mouse embryonic fibroblast
RFP	red fluorescent protein
SQSTM1/p62	sequestosome 1
TMA	tissue microarray
UPR	unfolded protein response
XBP1	x-box binding protein 1

ORCID

David Llobet-Navàs http://orcid.org/0000-0003-1443-7003

References

[1] Ferlay J, Shin HR, Bray F, Forman D, Mathers C, Parkin DM. Estimates of worldwide burden of cancer in 2008: GLOBOCAN 2008. Int J Cancer 2010; 127:2893-917; PMID:21351269; http://dx.doi.org/10.1002/ijc.25516

[2] Siegel RL, Miller KD, Jemal A. Cancer statistics, 2015. CA Cancer J Clin 2015; 65:5-29; PMID:25559415; http://dx.doi.org/10.3322/caac.21254

[3] Sorosky JI. Endometrial cancer. Obstet Gynecol 2012; 120:383-97; PMID:22825101; http://dx.doi.org/10.1097/AOG.0b013e3182605bf1

[4] Bokhman JV. Two pathogenetic types of endometrial carcinoma. Gynecol Oncol 1983; 15:10-7; PMID:6822361; http://dx.doi.org/10.1016/0090-8258(83)90111-7

[5] Kandoth C, Schultz N, Cherniack AD, Akbani R, Liu Y, Shen H, Robertson AG, Pashtan I, Shen R, Benz CC. Integrated genomic characterization of endometrial carcinoma. Nature 2013; 497:67-73.

[6] Nout RA, Smit VT, Putter H, Jurgenliemk-Schulz IM, Jobsen JJ, Lutgens LC, van der Steen-Banasik EM, Mens JW, Slot A, Kroese MC, et al. Vaginal brachytherapy versus pelvic external beam radiotherapy for patients with endometrial cancer of high-intermediate risk (PORTEC-2): an open-label, non-inferiority, randomised trial. Lancet 2010; 375:816-23; PMID:20206777; http://dx.doi.org/10.1016/S0140-6736(09)62163-2

[7] Blake P, Swart AM, Orton J, Kitchener H, Whelan T, Lukka H, Eisenhauer E, Bacon M, Tu D, Parmar MK. Adjuvant external beam radiotherapy in the treatment of endometrial cancer (MRC ASTEC and NCIC CTG EN.5 randomised trials): pooled trial results, systematic review, and meta-analysis. Lancet 2009; 373:137-46; PMID:19070891; http://dx.doi.org/10.1016/S0140-6736(08)61767-5

[8] Tangjitgamol S, See HT, Kavanagh J. Adjuvant chemotherapy for endometrial cancer. Int J Gynecol Cancer 2011; 21:885-95; PMID:21697679; http://dx.doi.org/10.1097/IGC.0b013e3182169239

[9] Fleming GF. Systemic chemotherapy for uterine carcinoma: metastatic and adjuvant. J Clin Oncol 2007; 25:2983-90; PMID:17617530; http://dx.doi.org/10.1200/JCO.2007.10.8431

[10] Gschwind A, Fischer OM, Ullrich A. The discovery of receptor tyrosine kinases: targets for cancer therapy. Nat Rev Cancer 2004; 4:361-70; PMID:15122207; http://dx.doi.org/10.1038/nrc1360

[11] Hunter T. The Croonian Lecture 1997. The phosphorylation of proteins on tyrosine: its role in cell growth and disease. Philos Trans R Soc Lond B Biol Sci 1998; 353:583-605; PMID:9602534; http://dx.doi.org/10.1098/rstb.1998.0228

[12] Knight ZA, Lin H, Shokat KM. Targeting the cancer kinome through polypharmacology. Nat Rev Cancer 2010; 10:130-7; PMID:20094047; http://dx.doi.org/10.1038/nrc2787

[13] Bruix J, Sherman M. Management of hepatocellular carcinoma: an update. Hepatology 2011; 53:1020-2; PMID:21374666; http://dx.doi.org/10.1002/hep.24199

[14] Escudier B, Eisen T, Stadler WM, Szczylik C, Oudard S, Siebels M, Negrier S, Chevreau C, Solska E, Desai AA, et al. Sorafenib in advanced clear-cell renal-cell carcinoma. N Engl J Med 2007; 356:125-34; PMID:17215530; http://dx.doi.org/10.1056/NEJMoa060655

[15] Wilhelm SM, Carter C, Tang L, Wilkie D, McNabola A, Rong H, Chen C, Zhang X, Vincent P, McHugh M, et al. BAY 43-9006 exhibits broad spectrum oral antitumor activity and targets the RAF/MEK/ERK pathway and receptor tyrosine kinases involved in tumor progression and angiogenesis. Cancer Res 2004; 64:7099-109; PMID:15466206; http://dx.doi.org/10.1158/0008-5472.CAN-04-1443

[16] Wilhelm S, Carter C, Lynch M, Lowinger T, Dumas J, Smith RA, Schwartz B, Simantov R, Kelley S. Discovery and development of sorafenib: a multikinase inhibitor for treating cancer. Nat Rev Drug Discov 2006; 5:835-44; PMID:17016424; http://dx.doi.org/10.1038/nrd2130

[17] Kamat AA, Merritt WM, Coffey D, Lin YG, Patel PR, Broaddus R, Nugent E, Han LY, Landen CN Jr, Spannuth WA, et al. Clinical and biological significance of vascular endothelial growth factor in endometrial cancer. Clin Cancer Res 2007; 13:7487-95; PMID:18094433; http://dx.doi.org/10.1158/1078-0432.CCR-07-1017

[18] McMeekin DS, Sill MW, Benbrook D, Darcy KM, Stearns-Kurosawa DJ, Eaton L, Yamada SD, Gynecologic Oncology Group. A phase II trial of thalidomide in patients with refractory endometrial cancer and correlation with angiogenesis biomarkers: a Gynecologic Oncology Group study. Gynecol Oncol 2007; 105:508-16; PMID:17306350; http://dx.doi.org/10.1016/j.ygyno.2007.01.019

[19] Ninomiya Y, Kato K, Takahashi A, Ueoka Y, Kamikihara T, Arima T, Matsuda T, Kato H, Nishida J, Wake N. K-Ras and H-Ras activation promote distinct consequences on endometrial cell survival. Cancer Res 2004; 64:2759-65; PMID:15087391; http://dx.doi.org/10.1158/0008-5472.CAN-3487-2

[20] Nimeiri HS, Oza AM, Morgan RJ, Huo D, Elit L, Knost JA, Wade JL 3rd, Agamah E, Vokes EE, Fleming GF. A phase II study of sorafenib in advanced uterine carcinoma/carcinosarcoma: a trial of the Chicago, PMH, and California Phase II Consortia. Gynecol Oncol 2010; 117:37-40; PMID:20117828; http://dx.doi.org/10.1016/j.ygyno.2010.01.013

[21] McDermott U, Sharma SV, Dowell L, Greninger P, Montagut C, Lamb J, Archibald H, Raudales R, Tam A, Lee D, et al. Identification of genotype-correlated sensitivity to selective kinase inhibitors by using high-throughput tumor cell line profiling. Proc Natl Acad Sci U S A 2007; 104:19936-41; PMID:18077425; http://dx.doi.org/10.1073/pnas.0707498104

[22] Subramanian A, Tamayo P, Mootha VK, Mukherjee S, Ebert BL, Gillette MA, Paulovich A, Pomeroy SL, Golub TR, Lander ES, et al. Gene set enrichment analysis: a knowledge-based approach for interpreting genome-wide expression profiles. Proc Natl Acad Sci U S A 2005; 102:15545-50; PMID:16199517; http://dx.doi.org/10.1073/pnas.0506580102

[23] Rahmani M, Davis EM, Bauer C, Dent P, Grant S. Apoptosis induced by the kinase inhibitor BAY 43-9006 in human leukemia cells involves down-regulation of Mcl-1 through inhibition of translation. J Biol Chem 2005; 280:35217-27; PMID:16109713; http://dx.doi.org/10.1074/jbc.M506551200

[24] Liu L, Cao Y, Chen C, Zhang X, McNabola A, Wilkie D, Wilhelm S, Lynch M, Carter C. Sorafenib blocks the RAF/MEK/ERK pathway, inhibits tumor angiogenesis, and induces tumor cell apoptosis in hepatocellular carcinoma model PLC/PRF/5. Cancer Res 2006; 66:11851-8; PMID:17178882; http://dx.doi.org/10.1158/0008-5472.CAN-06-1377

[25] Huynh H, Ngo VC, Koong HN, Poon D, Choo SP, Thng CH, Chow P, Ong HS, Chung A, Soo KC. Sorafenib and rapamycin induce growth suppression in mouse models of hepatocellular carcinoma. J Cell Mol Med 2009; 13:2673-83; PMID:19220580; http://dx.doi.org/10.1111/j.1582-4934.2009.00692.x

[26] Liu LP, Ho RL, Chen GG, Lai PB. Sorafenib inhibits hypoxia-inducible factor-1alpha synthesis: implications for antiangiogenic activity in hepatocellular carcinoma. Clin Cancer Res 2012; 18:5662-71; PMID:22929805; http://dx.doi.org/10.1158/1078-0432.CCR-12-0552

[27] Rosato RR, Almenara JA, Coe S, Grant S. The multikinase inhibitor sorafenib potentiates TRAIL lethality in human leukemia cells in association with Mcl-1 and cFLIPL down-regulation. Cancer Res 2007; 67:9490-500; PMID:17909059; http://dx.doi.org/10.1158/0008-5472.CAN-07-0598

[28] Rahmani M, Davis EM, Crabtree TR, Habibi JR, Nguyen TK, Dent P, Grant S. The kinase inhibitor sorafenib induces cell death through a process involving induction of endoplasmic reticulum stress. Mol Cell Biol 2007; 27:5499-513; PMID:17548474; http://dx.doi.org/10.1128/MCB.01080-06

[29] Rahmani M, Nguyen TK, Dent P, Grant S. The multikinase inhibitor sorafenib induces apoptosis in highly imatinib mesylate-resistant bcr/abl+ human leukemia cells in association with signal transducer and activator of transcription 5 inhibition and myeloid cell leukemia-1 down-regulation. Mol Pharmacol 2007; 72:788-95; PMID:17595328; http://dx.doi.org/10.1124/mol.106.033308

[30] Llobet D, Eritja N, Yeramian A, Pallares J, Sorolla A, Domingo M, Santacana M, Gonzalez-Tallada FJ, Matias-Guiu X, Dolcet X. The multikinase inhibitor Sorafenib induces apoptosis and sensitises endometrial cancer cells to TRAIL by different mechanisms. Eur J Cancer 2010; 46:836-50; PMID:20071162; http://dx.doi.org/10.1016/j.ejca.2009.12.025

[31] Sun NK, Huang SL, Chang TC, Chao CC. Sorafenib induces endometrial carcinoma apoptosis by inhibiting Elk-1-dependent Mcl-1 transcription and inducing Akt/GSK3beta-dependent protein degradation. J Cell Biochem 2013; 114:1819-31; PMID:23463670; http://dx.doi.org/10.1002/jcb.24530

[32] Hikita H, Takehara T, Shimizu S, Kodama T, Shigekawa M, Iwase K, Hosui A, Miyagi T, Tatsumi T, Ishida H, et al. The Bcl-xL inhibitor, ABT-737, efficiently induces apoptosis and suppresses growth of hepatoma cells in combination with sorafenib. Hepatology 2010; 52:1310-21; PMID:20799354; http://dx.doi.org/10.1002/hep.23836

[33] Rahmani M, Aust MM, Attkisson E, Williams DC, Jr., Ferreira-Gonzalez A, Grant S. Inhibition of Bcl-2 antiapoptotic members by obatoclax potently enhances sorafenib-induced apoptosis in human myeloid leukemia cells through a Bim-dependent process. Blood 2012; 119:6089-98; PMID:22446485; http://dx.doi.org/10.1182/blood-2011-09-378141

[34] Barretina J, Caponigro G, Stransky N, Venkatesan K, Margolin AA, Kim S, Wilson CJ, Lehár J, Kryukov GV, Sonkin D, et al. The Cancer Cell Line Encyclopedia enables predictive modelling of anticancer drug sensitivity. Nature 2012; 483:603-7; PMID:22460905; http://dx.doi.org/10.1038/nature11003

[35] Settembre C, Fraldi A, Medina DL, Ballabio A. Signals from the lysosome: a control centre for cellular clearance and energy metabolism. Nat Rev Mol Cell Biol 2013; 14:283-96; PMID:23609508; http://dx.doi.org/10.1038/nrm3565

[36] Parks SK, Chiche J, Pouyssegur J. Disrupting proton dynamics and energy metabolism for cancer therapy. Nat Rev Cancer 2013; 13:611-23; PMID:23969692; http://dx.doi.org/10.1038/nrc3579

[37] Kondo Y, Kanzawa T, Sawaya R, Kondo S. The role of autophagy in cancer development and response to therapy. Nat Rev Cancer 2005; 5:726-34; PMID:16148885; http://dx.doi.org/10.1038/nrc1692

[38] Shi YH, Ding ZB, Zhou J, Hui B, Shi GM, Ke AW, Wang XY, Dai Z, Peng YF, Gu CY, et al. Targeting autophagy enhances sorafenib lethality for hepatocellular carcinoma via ER stress-related apoptosis. Autophagy 2011; 7:1159-72; PMID:21691147; http://dx.doi.org/10.4161/auto.7.10.16818

[39] Luo T, Fu J, Xu A, Su B, Ren Y, Li N, et al. PSMD10/Gankyrin induces autophagy to promote tumor progression through cytoplasmic interaction with ATG7 and nuclear transactivation of ATG7 expression. Autophagy 2016; 12:1355-71; PMID:25905985; http://dx.doi.org/10.1080/15548627.2015.1034405

[40] Bareford MD, Park MA, Yacoub A, Hamed HA, Tang Y, Cruickshanks N, Eulitt P, Hubbard N, Tye G, Burow ME, et al. Sorafenib enhances pemetrexed cytotoxicity through an autophagy-dependent mechanism in cancer cells. Cancer Res 2011; 71:4955-67; PMID:21622715; http://dx.doi.org/10.1158/0008-5472.CAN-11-0898

[41] Tai WT, Shiau CW, Chen HL, Liu CY, Lin CS, Cheng AL, Chen PJ, Chen KF. Mcl-1-dependent activation of Beclin 1 mediates autophagic cell death induced by sorafenib and SC-59 in hepatocellular carcinoma cells. Cell Death Dis 2013; 4:e485; PMID:23392173; http://dx.doi.org/10.1038/cddis.2013.18

[42] Zhai B, Hu F, Jiang X, Xu J, Zhao D, Liu B, Pan S, Dong X, Tan G, Wei Z, et al. Inhibition of Akt reverses the acquired resistance to sorafenib by switching protective autophagy to autophagic cell death in hepatocellular carcinoma. Mol Cancer Ther 2014; 13:1589-98; PMID:24705351; http://dx.doi.org/10.1158/1535-7163.MCT-13-1043

[43] Klionsky DJ, Abdalla FC, Abeliovich H, Abraham RT, Acevedo-Arozena A, Adeli K, Agholme L, Agnello M, Agostinis P, Aguirre-Ghiso JA, et al. Guidelines for the use and interpretation of assays for monitoring autophagy. Autophagy 2012; 8:445-544; PMID:22966490; http://dx.doi.org/10.4161/auto.19496

[44] Gonzalez-Polo RA, Boya P, Pauleau AL, Jalil A, Larochette N, Souquere S, Eskelinen EL, Pierron G, Saftig P, Kroemer G. The apoptosis/autophagy paradox: autophagic vacuolization before apoptotic death. J Cell Sci 2005; 118:3091-102; PMID:15985464; http://dx.doi.org/10.1242/jcs.02447

[45] Kimura S, Noda T, Yoshimori T. Dissection of the autophagosome maturation process by a novel reporter protein, tandem fluorescent-tagged LC3. Autophagy 2007; 3:452-60; PMID:17534139; http://dx.doi.org/10.4161/auto.4451

[46] Baker BM, Chen CS. Deconstructing the third dimension: how 3D culture microenvironments alter cellular cues. J Cell Sci 2012; 125:3015-24; PMID:22797912; http://dx.doi.org/10.1242/jcs.079509

[47] Wiersma VR, de Bruyn M, Wei Y, van Ginkel RJ, Hirashima M, Niki T, Nishi N, Zhou J, Pouwels SD, Samplonius DF, et al. The epithelial polarity regulator LGALS9/galectin-9 induces fatal frustrated autophagy in KRAS mutant colon carcinoma that depends on elevated basal autophagic flux. Autophagy 2015; 11:1373-88; PMID:26086204; http://dx.doi.org/10.1080/15548627.2015.1063767

[48] Inamoto T, Azuma H. Sorafenib increases endoplasmic reticulum (ER) stress in concert with vorinostat. Cancer Biol Ther 2011; 12:1018; PMID:22095133; http://dx.doi.org/10.4161/cbt.12.12.18135

[49] Senft D, Ronai ZA. UPR, autophagy, and mitochondria crosstalk underlies the ER stress response. Trends Biochem Sci 2015; 40:141-8; PMID:25656104; http://dx.doi.org/10.1016/j.tibs.2015.01.002

[50] Kang KA, Kim JK, Jeong YJ, Na SY, Hyun JW. Dictyopteris undulata extract induces apoptosis via induction of endoplasmic reticulum stress in human colon cancer cells. J Cancer Prev 2014; 19:118-24; PMID:25337580; http://dx.doi.org/10.15430/JCP.2014.19.2.118

[51] Abdelrahim M, Newman K, Vanderlaag K, Samudio I, Safe S. 3,3′-diindolylmethane (DIM) and its derivatives induce apoptosis in pancreatic cancer cells through endoplasmic reticulum stress-dependent upregulation of DR5. Carcinogenesis 2006; 27:717-28; PMID:16332727; http://dx.doi.org/10.1093/carcin/bgi270

[52] Zhang R, Kim JS, Kang KA, Piao MJ, Kim KC, Hyun JW. Protective mechanism of KIOM-4 in streptozotocin-induced pancreatic beta-cells damage is involved in the inhibition of endoplasmic reticulum stress. Evid Based Complement Alternat Med 2011; 2011.

[53] B'Chir W, Maurin AC, Carraro V, Averous J, Jousse C, Muranishi Y, Parry L, Stepien G, Fafournoux P, Bruhat A. The eIF2alpha/ATF4 pathway is essential for stress-induced autophagy gene expression. Nucleic Acids Res 2013; 41:7683-99; PMID:23804767; http://dx.doi.org/10.1093/nar/gkt563

[54] Deegan S, Saveljeva S, Gorman AM, Samali A. Stress-induced self-cannibalism: on the regulation of autophagy by endoplasmic reticulum stress. Cell Mol Life Sci 2013; 70:2425-41; PMID:23052213; http://dx.doi.org/10.1007/s00018-012-1173-4

[55] Urano F, Wang X, Bertolotti A, Zhang Y, Chung P, Harding HP, Ron D. Coupling of stress in the ER to activation of JNK protein kinases by transmembrane protein kinase IRE1. Science 2000; 287:664-6; PMID:10650002; http://dx.doi.org/10.1126/science.287.5453.664

[56] Hagiwara S, Kudo M, Nagai T, Inoue T, Ueshima K, Nishida N, Watanabe T, Sakurai T. Activation of JNK and high expression level of CD133 predict a poor response to sorafenib in hepatocellular carcinoma. Br J Cancer 2012; 106:1997-2003; PMID:22596232; http://dx.doi.org/10.1038/bjc.2012.145

[57] Wang L, Gallo KA, Conrad SE. Targeting mixed lineage kinases in ER-positive breast cancer cells leads to G2/M cell cycle arrest and apoptosis. Oncotarget 2013; 4:1158-71; PMID:23902710; http://dx.doi.org/10.18632/oncotarget.1093

[58] Sweeney ZK, Lewcock JW. ACS chemical neuroscience spotlight on CEP-1347. ACS Chem Neurosci 2011; 2:3-4; PMID:22778853; http://dx.doi.org/10.1021/cn1000793

[59] Sinha S, Levine B. The autophagy effector Beclin 1: a novel BH3-only protein. Oncogene 2008; 27 Suppl 1:S137-48; PMID:19641499; http://dx.doi.org/10.1038/onc.2009.51

[60] Giatromanolaki A, Koukourakis MI, Koutsopoulos A, Chloropoulou P, Liberis V, Sivridis E. High Beclin 1 expression defines a poor prognosis in endometrial adenocarcinomas. Gynecol Oncol 2011; 123:147-51; PMID:21741077; http://dx.doi.org/10.1016/j.ygyno.2011.06.023

[61] Peng YF, Shi YH, Ding ZB, Ke AW, Gu CY, Hui B, Zhou J, Qiu SJ, Dai Z, Fan J. Autophagy inhibition suppresses pulmonary metastasis of HCC in mice via impairing anoikis resistance and colonization of HCC cells. Autophagy 2013; 9:2056-68; PMID:24157892; http://dx.doi.org/10.4161/auto.26398

[62] Deng L, Feng J, Broaddus RR. The novel estrogen-induced gene EIG121 regulates autophagy and promotes cell survival under stress. Cell Death Dis 2010; 1:e32; PMID:21072319; http://dx.doi.org/10.1038/cddis.2010.9

[63] Orfanelli T, Jeong JM, Doulaveris G, Holcomb K, Witkin SS. Involvement of autophagy in cervical, endometrial and ovarian cancer. Int J Cancer 2014; 135:519-28; PMID:24122662; http://dx.doi.org/10.1002/ijc.28524

[64] Lebovitz CB, Robertson AG, Goya R, Jones SJ, Morin RD, Marra MA, et al. Cross-cancer profiling of molecular alterations within the human autophagy interaction network. Autophagy 2015; 11:1668-87; PMID:26208877; http://dx.doi.org/10.1080/15548627.2015.1067362

[65] Sivridis E, Giatromanolaki A, Liberis V, Koukourakis MI. Autophagy in endometrial carcinomas and prognostic relevance of 'stone-like' structures (SLS): what is destined for the atypical endometrial hyperplasia? Autophagy 2011; 7:74-82; PMID:21099253; http://dx.doi.org/10.4161/auto.7.1.13947

[66] Johnson JI, Decker S, Zaharevitz D, Rubinstein LV, Venditti JM, Schepartz S, Kalyandrug S, Christian M, Arbuck S, Hollingshead M, et al. Relationships between drug activity in NCI preclinical in vitro and in vivo models and early clinical trials. Br J Cancer 2001; 84:1424-31; PMID:11355958; http://dx.doi.org/10.1054/bjoc.2001.1796

[67] Hidalgo M, Amant F, Biankin AV, Budinska E, Byrne AT, Caldas C, Clarke RB, de Jong S, Jonkers J, Mælandsmo GM, et al. Patient-derived xenograft models: an emerging platform for translational cancer research. Cancer Discov 2014; 4:998-1013; PMID:25185190; http://dx.doi.org/10.1158/2159-8290.CD-14-0001

[68] Brose MS, Nutting CM, Jarzab B, Elisei R, Siena S, Bastholt L, de la Fouchardiere C, Pacini F, Paschke R, Shong YK, et al. Sorafenib in radioactive iodine-refractory, locally advanced or metastatic differentiated thyroid cancer: a randomised, double-blind, phase 3 trial. Lancet 2014; 384:319-28; PMID:24768112; http://dx.doi.org/10.1016/S0140-6736(14)60421-9

[69] Llovet JM, Ricci S, Mazzaferro V, Hilgard P, Gane E, Blanc JF, de Oliveira AC, Santoro A, Raoul JL, Forner A, et al. Sorafenib in advanced hepatocellular carcinoma. N Engl J Med 2008; 359:378-90; PMID:18650514; http://dx.doi.org/10.1056/NEJMoa0708857

[70] Procopio G, Verzoni E, Testa I, Nicolai N, Salvioni R, Debraud F. Experience with sorafenib in the treatment of advanced renal cell carcinoma. Ther Adv Urol 2012; 4:303-13; PMID:23205057; http://dx.doi.org/10.1177/1756287212457216

[71] Zhai B, Sun XY. Mechanisms of resistance to sorafenib and the corresponding strategies in hepatocellular carcinoma. World J Hepatol 2013; 5:345-52; PMID:23898367; http://dx.doi.org/10.4254/wjh.v5.i7.345

[72] Shimizu S, Takehara T, Hikita H, Kodama T, Tsunematsu H, Miyagi T, Hosui A, Ishida H, Tatsumi T, Kanto T, et al. Inhibition of autophagy potentiates the antitumor effect of the multikinase inhibitor sorafenib in hepatocellular carcinoma. Int J Cancer 2012; 131:548-57; PMID:21858812; http://dx.doi.org/10.1002/ijc.26374

[73] Honma Y, Harada M. Sorafenib enhances proteasome inhibitor-mediated cytotoxicity via inhibition of unfolded protein response and keratin phosphorylation. Exp Cell Res 2013; 319:2166-78; PMID:23727131; http://dx.doi.org/10.1016/j.yexcr.2013.05.023

[74] Levine B, Kroemer G. Autophagy in the pathogenesis of disease. Cell 2008; 132:27-42; PMID:18191218; http://dx.doi.org/10.1016/j.cell.2007.12.018

[75] Allavena G, Carrarelli P, Del Bello B, Luisi S, Petraglia F, Maellaro E. Autophagy is upregulated in ovarian endometriosis: a possible interplay with p53 and heme oxygenase-1. Fertil Steril 2015; 103:1244-51e1; http://dx.doi.org/10.1016/j.fertnstert.2015.02.007

[76] Choi J, Jo M, Lee E, Oh YK, Choi D. The role of autophagy in human endometrium. Biol Reprod 2012; 86:70; PMID:22088918; http://dx.doi.org/10.1095/biolreprod.111.096206

[77] Zhang L, Liu Y, Xu Y, Wu H, Wei Z, Cao Y. The expression of the autophagy gene beclin-1 mRNA and protein in ectopic and eutopic endometrium of patients with endometriosis. Int J Fertil Steril 2015; 8:429-36; PMID:25780525

[78] Wei Y, Pattingre S, Sinha S, Bassik M, Levine B. JNK1-mediated phosphorylation of Bcl-2 regulates starvation-induced autophagy. Mol Cell 2008; 30:678-88; PMID:18570871; http://dx.doi.org/10.1016/j.molcel.2008.06.001

[79] Luo S, Garcia-Arencibia M, Zhao R, Puri C, Toh PP, Sadiq O, Rubinsztein DC. Bim inhibits autophagy by recruiting Beclin 1 to microtubules. Mol Cell 2012; 47:359-70; PMID:22742832; http://dx.doi.org/10.1016/j.molcel.2012.05.040

[80] Kenific CM, Thorburn A, Debnath J. Autophagy and metastasis: another double-edged sword. Curr Opin Cell Biol 2010; 22:241-5; PMID:19945838; http://dx.doi.org/10.1016/j.ceb.2009.10.008

[81] Herranz D, Ambesi-Impiombato A, Sudderth J, Sanchez-Martin M, Belver L, Tosello V, Xu L, Wendorff AA, Castillo M, Haydu JE, et al. Metabolic reprogramming induces resistance to anti-NOTCH1 therapies in T cell acute lymphoblastic leukemia. Nat Med 2015; 21:1182-9; PMID:26390244; http://dx.doi.org/10.1038/nm.3955

[82] Apel A, Herr I, Schwarz H, Rodemann HP, Mayer A. Blocked autophagy sensitizes resistant carcinoma cells to radiation therapy. Cancer Res 2008; 68:1485-94; PMID:18316613; http://dx.doi.org/10.1158/0008-5472.CAN-07-0562

[83] Bellodi C, Lidonnici MR, Hamilton A, Helgason GV, Soliera AR, Ronchetti M, Galavotti S, Young KW, Selmi T, Yacobi R, et al. Targeting autophagy potentiates tyrosine kinase inhibitor-induced cell death in Philadelphia chromosome-positive cells, including primary CML stem cells. J Clin Invest 2009; 119:1109-23; PMID:19363292; http://dx.doi.org/10.1172/JCI35660

[84] Shingu T, Fujiwara K, Bogler O, Akiyama Y, Moritake K, Shinojima N, Tamada Y, Yokoyama T, Kondo S. Stage-specific effect of

[85] Vazquez-Martin A, Oliveras-Ferraros C, Menendez JA. Autophagy facilitates the development of breast cancer resistance to the anti-HER2 monoclonal antibody trastuzumab. PLoS One 2009; 4:e6251; PMID:19606230; http://dx.doi.org/10.1371/journal.pone.0006251

[86] Garrido-Laguna I, Uson M, Rajeshkumar NV, Tan AC, de Oliveira E, Karikari C, Villaroel MC, Salomon A, Taylor G, Sharma R, et al. Tumor engraftment in nude mice and enrichment in stroma-related gene pathways predict poor survival and resistance to gemcitabine in patients with pancreatic cancer. Clin Cancer Res 2011; 17:5793-800; PMID:21742805; http://dx.doi.org/10.1158/1078-0432.CCR-11-0341

[87] Marangoni E, Vincent-Salomon A, Auger N, Degeorges A, Assayag F, de Cremoux P, de Plater L, Guyader C, De Pinieux G, Judde JG, et al. A new model of patient tumor-derived breast cancer xenografts for preclinical assays. Clin Cancer Res 2007; 13:3989-98; PMID:17606733; http://dx.doi.org/10.1158/1078-0432.CCR-07-0078

[88] Hidalgo M, Bruckheimer E, Rajeshkumar NV, Garrido-Laguna I, De Oliveira E, Rubio-Viqueira B, Strawn S, Wick MJ, Martell J, Sidransky D. A pilot clinical study of treatment guided by personalized tumorgrafts in patients with advanced cancer. Mol Cancer Ther 2011; 10:1311-6; PMID:21673092; http://dx.doi.org/10.1158/1535-7163.MCT-11-0233

[89] Eritja N, Llobet D, Domingo M, Santacana M, Yeramian A, Matias-Guiu X, Dolcet X. A novel three-dimensional culture system of polarized epithelial cells to study endometrial carcinogenesis. Am J Pathol 2010; 176:2722-31; PMID:20395448; http://dx.doi.org/10.2353/ajpath.2010.090974

[90] Cerami E, Gao J, Dogrusoz U, Gross BE, Sumer SO, Aksoy BA, Jacobsen A, Byrne CJ, Heuer ML, Larsson E, et al. The cBio cancer genomics portal: an open platform for exploring multidimensional cancer genomics data. Cancer Discov 2012; 2:401-4; PMID:22588877; http://dx.doi.org/10.1158/2159-8290.CD-12-0095

[91] Gao J, Aksoy BA, Dogrusoz U, Dresdner G, Gross B, Sumer SO, Sun Y, Jacobsen A, Sinha R, Larsson E, et al. Integrative analysis of complex cancer genomics and clinical profiles using the cBioPortal. Sci Signal 2013; 6:pl1; PMID:23550210; http://dx.doi.org/10.1126/scisignal.2004088

[92] Hubbell E, Liu WM, Mei R. Robust estimators for expression analysis. Bioinformatics 2002; 18:1585-92; PMID:12490442; http://dx.doi.org/10.1093/bioinformatics/18.12.1585

[93] Ashburner M, Ball CA, Blake JA, Botstein D, Butler H, Cherry JM, Davis AP, Dolinski K, Dwight SS, Eppig JT, et al. Gene ontology: tool for the unification of biology. The Gene Ontology Consortium. Nat Genet 2000; 25:25-9; PMID:10802651; http://dx.doi.org/10.1038/75556

[94] Burgess A, Vigneron S, Brioudes E, Labbe JC, Lorca T, Castro A. Loss of human Greatwall results in G2 arrest and multiple mitotic defects due to deregulation of the cyclin B-Cdc2/PP2A balance. Proc Natl Acad Sci U S A 2010; 107:12564-9; PMID:20538976; http://dx.doi.org/10.1073/pnas.0914191107

[95] McCloy RA, Rogers S, Caldon CE, Lorca T, Castro A, Burgess A. Partial inhibition of Cdk1 in G 2 phase overrides the SAC and decouples mitotic events. Cell Cycle 2014; 13:1400-12; PMID:24626186; http://dx.doi.org/10.4161/cc.28401